Development of carbon based optically transparent electrodes from pyrolyzed

photoresist for the investigation of phenomena at electrified carbon - solution interfaces

by

Sebastian Donner

A dissertation submitted to the graduate faculty

in partial fulfillment of the requirements for the degree of

DOCTOR OF PHILOSOPHY

Major: Analytical Chemistry

Program of Study Committee:
Marc Porter, Co-major Professor
Robert Houk, Co-major Professor
Emily Smith
Theresa Windus
Andrew Hillier

Iowa State University

Ames, Iowa

2007

DEDICATIONS AND ACKNOWLEDGEMENTS

This dissertation is dedicated to my wife, Jennifer Lynn Klages.

I give my thanks and deep appreciation to all the people that have made this dissertation possible. With gratitude I recognize the support and freedom offered by my major professor, Marc Porter. I would also like to thank the members of our research group throughout the years for collaborations, mutual exchange of knowledge, constructive criticism, encouraging words, and helpful conversations.

I thank collaborators Edward Yeung, Hung-Wing Li, and Jiangwei Li for helpful discussions, assistance with experiments, and the opportunity to learn about a variety of exciting topics and techniques in bioanalytical chemistry.

Most of all I thank my family for their support over the many years of personal and educational development. Foremost I am grateful for my wife Jennifer who always encouraged me and helped me broaden my horizon tremendously. I thank my mother, Christiane, for raising two talented boys; my father, Hubertus, who is always watching out for me; and my brother, Christoph, who has always been encouraging and believed in me.

Special thanks to the family of Steffen and Siegrun Kist, who have made my move from East Germany to West Germany possible and without whom I would not be in the US today. I also thank my host family Wade-Myers for a great year and introducing me the American Way of Life.

Table of Contents

ABSTRACT

The work presented herein describes fundamental investigations of carbon as electrode material by using the pyrolysis of photoresist to create an optically transparent material. The development of these carbon-based optically transparent electrodes (C-OTEs) enables investigations of molecular interactions within the electrical double layer, processes that are central to a wide range of important phenomena, including the impact of changes in the surface charge density on adsorption [1].

The electrochemical importance of carbon cannot be understated, having relevance to separations and detection by providing a wide potential window and low background current in addition to being low cost and light weight [2, 3]. The interactions that govern the processes at the carbon electrode surface has been studied extensively[2, 3]. A variety of publications from the laboratories of McCreery and Kinoshita provide in depth summaries about carbon and its many applications in electrochemistry.[2-4] These studies reveal that defects, impurities, oxidation, and a variety of functional groups create adsorption sites on carbon surfaces with different characteristics [1-4].

Our interest in C-OTEs was sparked by the desire to study and understand the behavior of individual molecules at electrified interfaces. It draws on our earlier development of Electrochemically Modulated Liquid Chromatography (EMLC) [5-10], which uses carbon as the stationary phase. EMLC takes advantage of changing the applied potential to the carbon electrode to influence the retention behavior of analytes. However, perspectives gained from, for example, chromatographic measurements reflect the integrated response of a large ensemble of potentially diverse interactions between the adsorbates and the carbon electrode. Considering the chemically and physically heterogeneous surface of electrode materials such as glassy carbon [3, 11], the integrated response provides little insight into the interactions at

a single molecule level. To investigate individual processes, we have developed C-OTEs in order to couple electrochemistry with single molecule spectroscopy (SMS).

Like EMLC, the novel merger of SMS with electrochemistry is a prime example of how a hybrid method can open new and intriguing avenues that are of both fundamental and technological importance. We show that by taking the benefits of total internal reflection fluorescence microscopy (TIRFM) and incorporating carbon as electrode material observations central to the interactions between single DNA molecules and an electrified carbon surface can be delineated.

Using TIRFM while applying a positive potential to the electrode, individual molecules can be observed as they reversibly and irreversibly adsorb to the carbon surface. The positive potential attracts the negatively charged DNA molecules to the electrode surface. Dye labels on the DNA within the evanescent wave are excited and their fluorescence is captured by an intensified charge coupled device (ICCD) camera. Results are therefore presented regarding the interactions of λ-DNA, 48,502 base pairs (48.5 kbp), HPV-16, 7.9 kbp, and a 1 kbp fraction of pBR322 DNA. In addition to the influence of molecular size on adsorption, the fabrication, characterization, and more conventional spectroelectrochemical applications of these novel C-OTEs are presented.

CHAPTER 1. GENERAL INTRODUCTION

Dissertation Organization

The work presented herein is driven in large part by our interest in occurrences at the molecular level that govern the performance of electrochemically modulated liquid chromatography (EMLC). Advanced in the early 1990's by the Porter research group, EMLC takes advantage of altering the surface charge density at the carbon-solution interface to fine-tune the retention of a wide range of molecules like aromatic sulfonates[7, 12], corticosteroids[13], benzodiazepines[8], and barbiturates[14]. The research herein seeks to unravel the influence of the applied potential on the carbonaceous materials on the sorptive interactions with complex samples by combining optically transparent carbon electrodes and single molecule spectroscopy.

This dissertation is separated into five chapters. This chapter provides a general description of the concepts used and background needed to place the following research sections in perspective. Chapters two and three discuss the development and characterization of the carbon based optically transparent electrodes (C-OTEs) and their applicability for single molecule spectroelectrochemistry.

Chapter two focuses on the fabrication of C-OTEs using positive photoresist AZ 4330 RS as the starting material. Chapter three describes the development and advantages of C-OTEs that use the negative photoresist SU-8 2000.5 as the precursor. While Chapter two addresses the issue of single molecule detection, it also lays the groundwork for the third chapter. The focus of Chapter three is the detection of individual, fluorescently tagged DNA molecules during adsorption under the influence of an applied potential.

Some of the key findings indicate that the overall negatively charged DNA molecules often bind irreversibly to the carbon surface at positive applied potentials, and then do not desorb upon application of a negative potential. When switching the applied potential from a negative to a positive value, negatively charged DNA molecules appear to move away from the surface initially before then being attracted to the surface. Variations in the size of the molecules were also examined to probe the influence of molecular size on the effectiveness of attractive and repulsive forces at different applied potentials.

Chapter four presents an alternative approach to the fabrication of the electrodes described in the previous chapters. Taking advantage of patterning small structures prior to pyrolysis allows the creation of carbon grid optically transparent electrodes (CG-OTEs). Combining the ability to change the patterns and dimensions of the grid electrodes photolithographically with the maintenance of the patterned shape throughout pyrolysis enables the manufacture of complex minigrid electrodes. The fourth chapter describes the fabrication and characterization of these CG-OTEs.

Chapter five provides conclusions as well as an outlook to potential research relating to C-OTEs and CG-OTEs. Citations of literature referenced are listed at the end of each chapter. While related to each other, Chapters two through five can stand-alone and have been or are intended to be published separately in scientific, peer-reviewed journals.

1. General Overview

EMLC has been a successful combination of electrochemistry and chromatography [10]. The key feature is the use of a conductive carbon stationary phase that also serves as a working electrode [6, 10]. Traditional liquid chromatography (LC) systems rely on the

interaction of a specific stationary phase with the analyte and solvent molecules, with retention governed largely by the composition of the stationary and mobile phases [15]. EMLC adds the ability to manipulate the impact of electrostatic attraction/repulsion on retention. Inducing a change in surface charge density of the stationary phase will therefore influence the attractive/repulsive behavior of both analyte and mobile phase components, leading to a change in elution time [10].

Traditionally, the development of retention mechanisms in LC is based on the average of many individual interactions that occur between the stationary phase, analyte and solvent. These theories are therefore based on what occurs from an integration of the interactions for a larger number of molecules, but not generally constructed from actual observation of single molecule interactions. However, to fully probe what occurs at the surface of the carbon stationary phase, it is important to visualize and observe events molecule-by-molecule.

In order to enable such observations, we have attempted and succeeded in fabricating optically transparent carbon electrodes, noting that most of the reports on EMLC have employed porous graphitic carbon as a stationary phase. Using the commercially available photoresist that has been used by others to fabricate thick-film carbon electrodes [16-20], we were able to modify existing protocols to prepare pyrolyzed carbon films that are thin enough to be transparent while maintaining electrical conductivity [1].

The fabrication of C-OTEs by pyrolization of photoresist is a fairly recent occurrence, and a great amount of research was necessary to evaluate and characterize the electrochemical performance, as well as the physical and chemical properties of the resulted material. We have therefore evaluated these new electrodes, for example, with cyclic voltammetry, chronoabsorptometry, 4-point probe conductivity, atomic force microscopy

(AFM), scanning electron microscopy (SEM), UV-vis spectroscopy, X-ray photon spectroscopy (XPS), and Raman spectroscopy.

In addition to the material characterization, the C-OTEs were successfully applied in single molecule spectroelectrochemistry (SMSEC) by combining the electrochemical applicability with total internal reflection fluorescence microscopy (TIRFM). The transparency of the electrode allows the evanescent wave to protrude beyond the C-OTE and into solution enabling the fluorescence of dye labeled molecules that are within ~130 nm of the surface. Spectroscopic detection can then be used to probe how the attraction of charged molecules to the electrode surface is affected by changes in the potential applied to C-OTEs.

2. Optically Transparent Electrodes

History. The first publication describing the concept of optically transparent conductive films in 1884 by Fritts[21] sparked scientific endeavors that have led to wide ranging applications in today's world. Coating thin films of gold[21], silver[22], or platinum[23] on selenium photoelectric cells were the earliest reported applications of conductive transparent coatings [24].

The first commercial usage of transparent conductive coatings involved solid-state photodetectors made with copper oxide [25] or selenium cells with metal coatings [26]. The most common preparation method for these films in the 1930s was by sputter coating metals like gold or silver [27].

The development of wide-band-gap semiconductor films like tin oxide in the 1940s broadened the range of OTE-applications [28]. The ability to spray the conductive transparent material facilitated the manufacture of commercial products like Nesa glass. The

development of indium oxide [29], tin oxide[30], and cadmium oxide [31] coatings started in the 1950s, but did not enter the commercial market until the 1960s [32].

Kuwana, Darlington, and Leedy introduced the concept of utilizing semiconductive coatings like the tin oxide in spectroelectrochemical experiments [33]. Described as a conducting glass electrode (CGE) at the time, the application of transparent and conductive coatings quickly gained acceptance for the investigation of optically absorbing electroactive species and their intermediates and products. Kuwana and colleagues [34-41], as well as other research teams [42], continued the development of optically transparent electrodes not only with transparent coatings, but also with the use of minigrid electrodes[43-45], which consist of a fine mesh (i.e., microscreen) of metal.

Minigrid OTEs can have several potential advantages over thin film OTEs. The optical transmission of minigrid OTEs is dependent on the perforations of the grid, and not on the electrode material itself [45]. Minigrid electrodes possess the same characteristics as their bulk material, minimizing issues resulting from thin film preparation like island formation and the internal ohmic resistance due to the nucleation and growth mechanism of metal thin films [24, 46-48].

Applications. From transmission spectroelectrochemistry to aircraft windows, OTEs have made a market for themselves. OTEs are used in imaging devices, can be found on aircraft windows for de-icing and de-fogging, provide electroluminescent lamps and displays, and serve as antistatic coatings on instrument panels. Transparent oxide electrodes are also components of modern liquid-crystal [49] and electrochromic [50] displays.

OTE Types. Taking the various applications into consideration, it should be apparent that different types of OTEs are needed for different applications. Striking a

balance between conductivity, transparency, and surface characteristics is therefore crucial, and matching material properties to the target application has become a major research endeavor.

Spectroelectrochemical experiments utilize a variety of OTEs. While transparent oxide electrodes are widely used, researchers also take advantage of thin film and grid electrodes that are composed of metals including gold, platinum, nickel, and silver [24, 45]. Numerous conducting, semimetallic, and semiconducting electrode materials have been investigated [47, 51-53].

Our current investigation focuses on the fabrication of carbon-based OTEs. Several attempts have been made to create such electrodes. The resistive sputtering and vapor deposition [53, 54] of carbon, as well as the pyrolysis of gases[55-59], organic thin films [60-62] and now photoresist [1] has been employed to create carbon-based OTEs. The latter adds the ability to photolithographically pattern OTEs.

Purpose. Carbon has been utilized as electrode material in numerous applications, including electroanalytical and electrosynthetic chemistry and energy conversion [2-4, 63, 64]. Enabling the manufacture of carbon electrodes that are optically transparent provides the opportunity to study the behavior of individual molecules as surface charge density is manipulated. Rendering carbon transparent allows incorporation of optical transformations concurrently with electrochemical (e.g., current) responses.

3. Pyrolyzing Photoresist Films

The fabrication of C-OTEs for the investigation of adsorption characteristics at electrified interfaces is based on creating thin (tens of nanometers) pyrolyzed photoresist films (PPF). Photoresist is commercially available with well-defined and very reproducible material characteristics. Positive photoresists, consisting of solvents and a novolak resin that increases in solubility upon UV light exposure, as well as negative, epoxy based photoresists where UV-exposure cross-links and hardens the polymer, are available in different viscosities. The viscosity determines the thickness of the film obtained through spin-coating the photoresist onto a substrate.

Recent research efforts by Kinoshita [18, 65], McCreery [16], and Madou [16, 18] yielded carbon electrodes that are prepared by pyrolyzing photoresist. Using several different photoresists, PPFs formed under various pyrolysis conditions were characterized. Investigations using Raman spectroscopy, X-ray photoelectron spectroscopy (XPS), Atomic Force Microscopy (AFM), 4-point electrical conductivity probes, and electrochemistry allowed optimization of this electrode material. This groundwork indicates that pyrolyzation at 1000 °C in a reducing atmosphere yields electrodes that are comparable in performance to glassy carbon electrodes.

Fabrication. A thin layer of photoresist is spin coated onto a suitable substrate. The pyrolysis temperature must be considered. Polished, doped silicon wafers are often used because, in addition to providing a smooth surface and temperature stability, they are more conductive than PPF and can decrease internal resistance between electrode contact and the carbon-solution interface.

For the fabrication of C-OTEs, a transparent substrate, quartz, is used to ensure that the resulting electrodes can be used in transmission SEC experiments [24]. There are two options for preparation of a film that is thin enough to be transparent after pyrolysis. One possibility is to dilute a positive photoresist (i.e. AZ 4330) in order to decrease the viscosity. To prepare, for example, a 35-nm thick C-OTE, AZ 4330 is mixed in a 1:2 ratio (33%) with 1-methoxy-2-propanol acetate. The other pathway is to use a photoresist that already has the desired viscosity. The negative photoresist SU 8-2000.5, when spin coated at the same rate as the dilute AZ 4330 solution (i.e., 6000 rpm for 30 s) and pyrolyzed at 1000 °C, will result in a C-OTE with a thickness of ~50 nm.

The pyrolysis conditions of choice include a reducing atmosphere consisting of 95% high purity nitrogen and 5% hydrogen, a composition that ensures minimization of oxygen during pyrolysis by yielding a hydrogen-terminated surface. This gas mixture is referred to as the forming gas. The Whitesides research group provides a detailed description of the events that occur throughout the pyrolysis process [20]. Below 300 °C solvent molecules and carbon mono- and dioxide are eliminated. Between 300 °C and 600 °C a rapid decrease in mass occurs while conjugated carbon networks that are electronically isolated form. These connect into a aromatic network above 600 °C, while cresols, phenols, and hydrocarbons are volatized [20].

The forming gas usually flows from the time at which the samples are introduced into the furnace until they are completely cooled after pyrolysis. At the end of the process, the furnace is flushed with 100% nitrogen to ensure the absence of hydrogen, which is a potential fire/combustion/explosion hazard.

Pyrolysis usually takes place in a furnace fitted with a quartz or hard-fired alumina tube. The flow rate of the forming gas depends on the diameter of the tube, and ranges between 100 and 1000 sccm. Characteristics of PPFs prepared with pyrolysis temperatures ranging from 600 °C to 1100 °C have been extensively investigated [1, 16-20, 65-67].

4. Material Evaluation

Numerous aspects of the PPFs have been characterized. Most important, the conductivity of these films has been measured with four-point probes. Four-point probes allow the determination of sheet resistance by applying a known current through the outer two of four equally spaced contacts, while measuring the voltage drop between the inner two contacts. Using Ohm's Law, we can determine the sheet resistance ($\Omega/\square$), which when combined with knowing the distance between the voltage-measuring contacts, can be employed to calculate the material resistivity and conductivity. For PPF, the resulting resistivity is $\sim 5 \times 10^{-3} \, \Omega/cm$ [1, 16].

The conductivity arises from the carbonization and formation of an extended aromatic network. The highly disordered amorphous material includes sp^2 and sp^3 graphite crystallites that are interconnected with sp^2 ribbons of carbon. Raman spectroscopy indicates that the network starts forming above 600 °C [16, 65]. To achieve conductivity adequate for our work, samples need to be pyrolyzed above 800 °C.

Thermogravimetric analysis (TGA) indicates that the largest decrease in film thickness occurs prior to reaching 600 °C. PPF pyrolyzed at 1000 °C displays an 80% loss in film thickness when compared to unpyrolyzed photoresist [16]. Patterned, micron-sized

features exhibit large vertical shrinkages, but little lateral shrinkage, which is another attractive feature of photoresist as starting material [16, 19].

Several microscopy techniques can be utilized to characterize PPF. Atomic force microscopy (AFM) can determine the smoothness, and sometimes thickness, of the pyrolyzed films [1, 16]. For films that are thicker than 100 nm the use of a profilometer or scanning electron microscope (SEM) to measure the film thickness is recommended. Both AFM and SEM provide a detailed view of PPF topography, which lacks observable porosity [16, 65]. Transmission electron microscopy (TEM) of small PPF samples can detail graphite structures embedded in the amorphous carbon film and substantiate the Raman findings [16].

XPS can provide information about the material composition. Analysis with XPS indicates that the oxygen content decreases with increasing pyrolysis temperature. The oxygen/carbon ratio stabilizes above 1000 °C [16]. While the oxygen content is 1.2% immediately after pyrolysis for a 1000 °C sample, the content slowly increases over a period of three days after which the oxygen and carbon contents stabilize at 3% and 97% respectively [1, 16].

5. Electrochemical Characterization

To substantiate the claim that PPF is an applicable electrode material, several electrochemical experiments can be performed. Cyclic voltammetry (CV) indicates that redox reactions with PPF electrodes proceed at rates comparable to that of most carbon electrodes. That is, CV investigations of the behavior of ruthenium hexamine $(Ru(NH_3)_6^{3+/2+})$ [16], hydroxylmethyl ferrocene ($FcCH_2OH$) [1], and ferrocyanide $(Fe(CN)_6^{3+/2+})$ redox couples [1] indicate that PPF formed at or above 1000 °C exhibits

characteristics similar to glassy carbon (GC) [16]. GC is the most utilized type of carbon electrode material, and is also both chemically and physically heterogeneous [3, 11].

The utilization of thin PPF to manufacture C-OTEs also requires transparency. The electrochemical behavior must therefore be tested in a transmission spectroelectrochemical experiment. Using the ferrocyanide redox couple, and knowing that the maximum absorption of ferricyanide occurs at 420 nm, the performance in a SEC cell can be evaluated. Applying a positive potential of +600 mV to the C-OTE causes the ferrocyanide originally in the SEC cell to oxidize to ferricyanide. The results from the ferrocyanide redox couple demonstrate that the transparent electrode material maintains the needed conductivity by showing that the rate of reactions is controlled by semi-infinite linear diffusion (SILD). Plotting the square root of time versus the absorbance change as ferrocyanide is oxidized to ferricyanide yields a linear plot, indicating that the rate of reactions during the SEC experiments with C-OTEs are controlled by SILD.

6. Single Molecule Spectroelectrochemistry

An exciting demonstration for the applicability of C-OTEs is the single molecule spectroelectrochemical (SMSEC) experiment [1]. Being able to observe individual molecules as they interact with a carbon electrode at different surface charge densities brings us to our original goal. Conclusions drawn from these observations will enable us to enhance our understanding of the interactions between the carbon surface and the analyte and solvent molecules that occur in EMLC.

SMS is different from conventional spectroscopy in a very basic fashion. Instead of averaging the response of an ensemble of molecules, SMS detects individual molecules

without averaging the results [68]. This capability provides information about specific molecule-surface interactions. SMS is especially useful for heterogeneous samples by identifying different processes at different locations within one sample [68-71].

The sensitivity of SMS to chronological changes is another advantage. It is possible to track the movement of individual molecules over time. For our purposes, distinct events can be quantified to gain insight about the heterogeneity of carbon. Valuable information can be obtained just as SMS has provided insights to biophysics [72-86], biochip [87-90] and biosensor [91-93] designs, molecular genetics[94-96], and separation theories of liquid chromatography and capillary electrophoresis [97-104].

The most popular mode of SMS uses fluorescence imaging [105]. Minimizing the number of molecules in the interrogation window and maintaining an acceptable signal-to-noise ratio (SNR) is vital [69]. Photobleaching the buffer solution, controlling the laser power, and minimizing exposure time are three active measures that can be used to maximize the SNR. Numerous instrumentation considerations exist to reduce noise, including the use of holographic notch attenuation filters, low fluorescence glass filters, interference filters, or the elimination of the excitation wavelength from the detector [106].

The utilization of TIRFM, also referred to as evanescent wave microscopy, represents another important component of the SMS measurement [106]. The total internal reflection (TIR) is the mechanism by which data are transmitted through fiber optic networks [106]. In TIR, optical radiation passes through a high refractive index material such as glass. When the beam encounters a low refractive index material, it is internally reflected if the incidence angle exceeds the critical angle [106].

While the radiation is reflected and does not travel through the second, low refractive index material, an electromagnetic field is created within a few hundred nanometers past the low refractive index material. This electromagnetic field, called the evanescent wave, has the same wavelength as the source radiation. Fluorescent molecules within the evanescent wave can then be excited and detected.

In the cases presented herein, the molecules of interest (DNA of various lengths) are labeled with a fluorescent dye. Upon laser excitation, labeled DNA within the evanescent wave in turn fluoresce. This fluorescence is captured and imaged as a function of time by an ICCD. Observing the response visually and knowing the electrochemical manipulation performed with the C-OTE allows us to interpret the phenomenon taking place at the electrified electrode-solution interface.

The following chapters present intriguing data and interpretations about the behavior of single molecules residing in the electrical double layer. Detailing the importance of molecular size and its affect on adsorption on carbon electrodes is made possible by the novel fabrication of C-OTEs and the merger of electrochemistry with single molecule spectroscopy. Temporal resolution of the adsorption process allows us to gain valuable information about molecular interactions and the heterogeneity of carbon.

7. References

[1]   S. Donner, H.-W. Li, E.S. Yeung and M.D. Porter, Analytical Chemistry, 78 (2006) 2816.
[2]   R.L. McCreery, in A.J. Bard (Editor), Electroanalytical Chemistry, Vol. 17, Marcel Dekker, New York, 1991, p. 221.
[3]   R.L. McCreery, in A. Wieckowski (Editor), Interfacial Electrochemistry, Marcel Dekker, Inc., New York, 1999, p. 631.
[4]   K. Kinoshita, Carbon: Electrochemical and Physiochemical Properties, Wiley, New York, 1988.

[5]   R.S. Deinhammer, M.D. Porter and K. Shimazu, Journal of Electroanalytical Chemistry, 387 (1995) 35.

[6]   R.S. Deinhammer, E.-Y. Ting and M.D. Porter, Journal of Electroanalytical Chemistry, 362 (1993).

[7]   E.-Y. Ting and M.D. Porter, Journal of Electroanalytical Chemistry, 443 (1998) 180.

[8]   E.-Y. Ting and M.D. Porter, Journal of Chromatography A, 793 (1998) 204.

[9]   R.S. Deinhammer, K. Shimazu and M.D. Porter, Analytical Chemistry, 63 (1991) 1889.

[10] J.A. Harnisch and M.D. Porter, Analyst, 126 (2001) 1841.

[11] J.P. Randin and E. Yeager, Electroanalytical Chemistry and Interfacial Electrochemistry, 58 (1975) 313.

[12] E.-Y. Ting and M.D. Porter, Analytical Chemistry, 70 (1998).

[13] E.-Y. Ting and M.D. Porter, Analytical Chemistry, 69 (1997).

[14] M. Ho, S. Wang and M.D. Porter, Analytical Chemistry, 70 (1998).

[15] A. Weston and P. Brown, R., High Performance Liquid Chromatography & Capillary Electrophoresis: Principles and Practices, Academic Press, San Diego, 1997.

[16] S. Ranganathan, R.L. McCreery, S.M. Majji and M. Madou, Journal of The Electrochemical Society, 147 (2000) 277.

[17] N.E. Hebert, B. Snyder, R.L. McCreery, W.G. Kuhr and S.A. Brazill, Analytical Chemistry, 75 (2003) 4265.

[18] J. Kim, X. Song, K. Kinoshita, M. Madou and R. White, Journal of the Electrochemical Society, 145 (1998) 2314.

[19] B.Y. Park, L.H. Taherabadi, C. Wang, J. Zoval and M. Madou, Journal of The Electrochemical Society, 152 (2005) J136.

[20] O.J.A. Schueller, S.T. Brittain and G.M. Whitesides, Sensors and Actuators A, 72 (1999) 125.

[21] C.E. Fritts, Proceedings of the American Association of Advanced Science, 33 (1884) 97.

[22] C. Bidwell, Philosophical Magazine, 20 (1885) 178.

[23] W. Von Uljanin, Ann. Phys. Leipzig, 34 (1888) 241.

[24] G. Haacke, Annual Review of Material Science, 7 (1977) 73.

[25] B. Lange, Phys. Z., 31 (1930) 964.

[26] L. Bergmann, Physical Z, 32 (1931) 286.

[27] E. Duhme and W. Schottky, Naturwissenschaften, 18 (1930) 735.

[28] Patent, 632256, 1942.

[29] Patent, 2516663, US, 1950.

[30] J.W. Ward, Appl. Ind., 16 (1955) 408.

[31] G. Helwig, Z. Phys., 132 (1952) 621.

[32] F.H. Gillery, Inf. Disp., 9 (1972) 17.

[33] T. Kuwana, R.K. Darlington and D.W. Leedy, Analytical Chemistry, 36 (1964) 2023.

[34] J.W. Strojek and T. Kuwana, Electroanalytical Chemistry, 16 (1968) 471.

[35] T. Osa and T. Kuwana, ibid, 22 (1969) 389.

[36] T. Kuwana and J.W. Strojek, Discussions of the Faraday Society, 45 (1968) 134.

[37] J.W. Strojek, G.A. Gruver and T. Kuwana, Analytical Chemistry, 41 (1969) 481.

[38] J.W. Strojek, T. Kuwana and S.W. Feldberg, American Chemical Society, 90 (1968) 1353.

[39] N. Winograd, H.N. Blount and T. Kuwana, Journal of Physical Chemistry, 73 (1969) 3456.

[40] G.C. Grant and T. Kuwana, Journal of Electroanalytical Chemistry 24 (1970) 11.

[41] W. von Benken and T. Kuwana, Analytical Chemistry, 43 (1971) 1114.

[42] B.S. Pons, J.S. Mattson, L.O. Winstrom and H.B. Mark, Analytical Chemistry, 39 (1967) 685.

[43] R.W. Murray, W.R. Heineman and G.W. O'Dom, Analytical Chemistry, 39 (1967) 1666.

[44] W.R. Heineman, J.N. Burnett and R.W. Murray, ibid, 40 (1968) 1970.

[45] M. Petek, T.E. Neal and R.W. Murray, Analytical Chemistry, 43 (1971) 1069.

[46] R.S. Sennet and G.D. Scott, Journal of the Optical Society of America, 40 (1950) 203.

[47] J.S. Mattson and C.A. Smith, Analytical Chemistry, 47 (1975) 1122.

[48] I. Levchenko and O. Baranov, Vacuum, 72 (2004) 205.

[49] G.H. Heilmeier, L.A. Zanoni and L.A. Barton, Applied Physics Letters, 13 (1968) 46.

[50] R.D. Giglia, International Symposium Coc. Inf. Disp. Wash. DC, 1975, p. 52.

[51] H.O. Finklea, R.K. Boggess, J.W. Trogdon and F.A. Schultz, Analytical Chemistry, 55 (1983) 1177.

[52] S. Haymond, J.K. Zak, Y. Show, J.E. Butler, G.T. Babcock and G.M. Swain, Analytical Chimica Acta, 500 (2003) 137.

[53] T.P. DeAngelis, R.W. Hurst, A.M. Yacynych, H.B. Mark, W.R. Heineman and J.S. Mattson, Analytical Chemistry, 49 (1977) 1395.

[54] J.C. Dawson and C.J. Adkins, Journal of Physics: Condensed Matter, 7 (1995) 6297.

[55] K. Lundstrom, Analytical Chimica Acta, 146 (1983).

[56] A.L. Beilby and A. Carlsson, Jounal of Electroanalytical Chemistry, 248 (1988).

[57] C.F. McFadden, L.L. Russel, P.R. Melaragno and J.A. Davis, Analytical Chemistry, 62 (1990).

[58] J.K. Clark, W.A. Schilling, C.A. Wijayawardhana and P.R. Melaragno, Analytical Chemistry, 66 (1994).

[59] R.A. Saraceno, C.E. Engstom, M. Rose and A.G. Ewing, Analytical Chemistry, 61 (1989).

[60] D.M. Anjo, S. Brown and W. Wang, Analytical Chemistry, 65 (1993) 317.

[61] O. Niwa and H. Tabel, Analytical Chemistry, 66 (1994).

[62] A. Rojo, A. Rosenstratten and D. Anjo, Analytical Chemistry, 58 (1986).

[63] R.L. McCreery, K.K. Ckine, C.A. McDermott and M.T. McDermott, Colloids and Surfaces, 93 (1994) 211.

[64] R.L. McCreery, in W.R. Kissinger and W.R. Heineman (Editors), Laboratory Techniques in Electroanalytical Chemistry, 2nd ed., Marcel Dekker, New York, 1996.

[65] R. Kostecki, B. Schnyder, D. Alliata, X. Song, K. Kinoshita and R. Koetz, Thin Solid Films, 396 (2001) 36.

[66] S. Ranganathan and R.L. McCreery, Analytical Chemistry, 73 (2001) 893.

[67] D. Fisher, J., W. Vandaveer IV, R., R. Grigsby, J. and S. Lunte, M., Electroanalysis, 17 (2005) 1153.

[68]   Y.J. Jung, E. Barkai and R.J. Silbey, Journal of Chemical Physics, 117 (2002) 10980.

[69]   W.E. Moerner, The Journal of Physical Chemistry B, 106 (2002) 910.

[70]   H.W. Li, H.Y. Park, M.D. Porter and E.S. Yeung, Analytical Chemistry, 77 (2005) 3256.

[71]   H.-Y. Park, H.-W. Li, E. Yeung, S. and M. Porter, D., Langmuir, 22 (2006) 4244.

[72]   A. Bensimon, A. Simon, A. Chiffaudel, V. Corquette, F. Heslot and D. Bensimon, Science, 265 (1994) 2096.

[73]   D. Bensimon, A.J. Simon, V. Corquette and A. Bensimon, Physical Review Letters, 74 (1995) 4754.

[74]   Q. Xue and E.S. Yeung, Nature, 373 (1995) 681.

[75]   T.W. Houseal, C. Bustamante, R.F. Stump and M.F. Maestre, Biophysical Journal, 56 (1989) 507.

[76]   I. Auzanneau, C. Barreau and L. Salome, Comptes Rendus de l' Academie des Sciences Serie III: Sciences de la Vie, 316 (1993) 459.

[77]   T.R. Strick, J.F. Allemand, D. Bensimon and V. Corquette, Biophysical Journal, 74 (1998) 2016.

[78]   F. Fan and A.J. Bard, Science, 267 (1995) 871.

[79]   T. Funatsu, Y. Harada, M. Tokunaga, K. Saito and T. Yanagida, Nature, 374 (1995) 555.

[80]   D.T. Chiu and R.N. Zare, Journal of the American Chemical Society, 118 (1996) 6512.

[81]   S. Nie, D.T. Chiu and R.N. Zare, Science, 266 (1994) 1018.

[82]   H. Yokota, K. Saito and T. Yanagida, Physical Review Letters, 80 (1998) 4606.

[83]   J. Enderlein, Biophysical Journal, 78 (2000) 2151.

[84]   X. Xu and E.S. Yeung, Science, 275 (1997) 1106.

[85]   R.M. Dickson, D.J. Norris, Y.L. Tzeng and W.E. Moerner, Science, 274 (1996) 966.

[86]   Y. Ma, M.R. Shortreed and E.S. Yeung, Analytical Chemistry, 72 (2000) 4640.

[87]   E.K. Hill and A.J. DeMello, Analyst, 125 (2000) 1033.

[88]   S.W.P. Turner, M. Levene, J. Korlach, W.W. Webb and D.J. Graves, Journal of Colloid and Interface Science, 203 (1998) 197.

[89]   B. Yoshinobu, 467-472 (2000).

[90]   G.V. Shivashankar and A. Libchaber, Current Science, 76 (1999) 813.

[91]   V. Chan, S.E. McKenzie, S. Surrey, P. Fortina and D.J. Graves, Journal of Colloid and Interface Science, 203 (1998) 197.

[92]   V. Chan, D.J. Graves, P. Fortina and S.E. McKenzie, Langmuir, 13 (1997) 320.

[93]   C.E. Jordan, A.G. Frutos, A.J. Thiel and R.M. Corn, Analytical Chemistry, 69 (1997) 4939.

[94]   J. Herrick, X. Michalet, C. Conti, C. Schurra and A. Bensimon, Proceedings of the National Academy of Sciences (USA), 97 (2000) 222.

[95]   J. Herrick and A. Bensimon, Chromosome Research, 7 (1999) 409.

[96]   Y.L. Lyubshenko and L.S. Shlyakhtenko, Proceedings of the National Academy of Sciences (USA), 94 (1997) 496.

[97]   X.H. Xu and E.S. Yeung, Science, 281 (1998) 1650.

[98]   M.R. Shortreed, H. Li, W.H. Huang and E.S. Yeung, Analytical Chemistry, 72 (2000) 2879.

[99]   S.B. Smith, P.K. Aldridge and J.B. Callis, Science, 243 (1989) 203.

[100]   M. Ueda, Journal of Biochemical and Biophysical Methods, 41 (1999) 153.

[101]   S.H. Kang, M.R. Shortreed and E.S. Yeung, Analytical Chemistry, 73 (2001) 1091.

[102]   J. Zheng and E.S. Yeung, Analytical Chemistry, 74 (2002) 4536.

[103]   S.H. Kang and E.S. Yeung, Analytical Chemistry, 74 (2002) 6334.

[104]   J. Zheng, H.W. Li and E.S. Yeung, Journal of Physical Chemistry, (2004).

[105]   E.S. Yeung, Annuual Review of Physical Chemistry, 55 (2004) 97.

[106]   H.-W. Li, Real-time monitoring and manipulation of single bio-molecules in free solution, Chemistry, Vol. Ph.D., Iowa State University, Ames, 2005.

CHAPTER 2. FABRICATION OF OPTICALLY TRANSPARENT CARBON ELECTRODES BY THE PYROLYSIS OF PHOTORESIST FILMS: APPROACH TO SINGLE-MOLECULE SPECTROELECTROCHEMISTRY

Sebastian Donner, Hung-Wing Li, Edward S. Yeung, and Marc D. Porter

Abstract

This paper describes the preparation, physical and chemical characterization, and performance of carbon-based optically transparent electrodes (C-OTEs) fabricated by the pyrolysis of thin films of photoresist. The electrodes are prepared by spin coating dilute solutions of the positive photoresist AZ 4330 onto quartz substrates. Pyrolysis of these samples at 1000°C in a reducing atmosphere yields optically transparent carbon films that have thicknesses ranging between 10 and 80 nm. Sheet resistance measurements, X-ray photoelectron spectroscopy, Raman spectroscopy, and atomic force microscopy were used to determine the physical and chemical properties of the films, and cyclic voltammetry and chronoabsorptometry were employed to delineate the electrochemical and conventional spectroelectrochemical performance of the C-OTEs. These findings showed that the transparency of this material improves as film thickness decreases, but at the expense of an increase in film resistance. At a wavelength of 500 nm, for example, 13- and 79-nm thick films have transparencies of 47% and 10% and sheet resistances of 1100 and 210 $\Omega/\square$, respectively. Importantly, adjusting the dilution factor allows the facile and reproducible variation of thickness and transparency. Preliminary results using these C-OTEs for single molecule spectroelectrochemistry, which represent a new development in the merger of

optical and electrochemical techniques, by probing the potential dependence of the adsorption of individual YOYO-I labeled λ–DNA are also presented.

1. Introduction

Optically transparent electrodes (OTEs) have proven invaluable to a wide range of investigations of electrochemical processes.[1-4] The design and synthesis of OTEs have traditionally relied on the deposition of conductive thin films like indium and tin oxide, gold, platinum, and to lesser extents, mercury, carbon, and doped diamond on a suitably transparent substrate.[1-8] Metallic microscreens, referred to as minigrid electrodes, have also been employed.[9] The vast majority of work on OTEs has focused on materials that can be applied in the visible region of the electromagnetic spectrum. In a few cases, however, access to infrared wavelengths has been achieved by either the deposition of germanium on an infrared transparent material[5] or the incisive doping of diamond film electrodes.[8]

The design of a film-based OTE represents a tradeoff between optical transparency and electrical resistivity, both of which are controlled by film thickness.[6] Film-based OTEs must be sufficiently thin, typically tens of nanometers, to be optically transparent. However, most electrode materials have large internal resistances at such thicknesses, which can distort the electrochemical response because of a distribution of the applied potential across the electrode surface. Thin film electrodes may also be mechanically fragile, posing handling problems.

This paper describes a novel approach to the facile fabrication of carbon-based OTEs (C-OTEs). Carbon is attractive as an electrode material because of its wide potential window, low background current, and low cost. Part of our interest in this area stems from the use of

carbon as a detector in sensor applications.[10] The work herein, however, was largely motivated by our continued development of electrochemically modulated liquid chromatography (EMLC).[11] EMLC is a form of high performance liquid chromatography in which the LC column is modified to also function as an electrochemical cell. The manipulation of the potential applied (E_{app}) to a conductive stationary phase like glassy carbon or porous graphitic carbon alters the surface charge density of the packing, which, in turn, fine tunes analyte retention.

In previous work, we have shown that measurements of retention with respect to changes in E_{app} can be employed to gain thermodynamic insights into the separation mechanism at carbonaceous packings.[12, 13] It follows that this type of measurement can also be exploited as a tool to probe fundamental issues central to adsorption at electrified interfaces. However, perspectives gained by such measurements reflect the integrated response of a large ensemble of analytes over a large, potentially diverse population of adsorption sites. Several studies have, in fact, amply demonstrated that the most used type of carbon electrode material, glassy carbon, has a surface that is both chemically and physically heterogeneous.[14, 15]

In an effort to probe adsorption at electrified interfaces on a much smaller length scale, this paper details the design, fabrication, and preliminary testing of C-OTEs suitable not only for conventional spectroelectrochemical applications, but also for investigations by single molecule spectroscopy. Earlier reports on the fabrication of C-OTEs have primarily employed the resistive sputtering and vapor deposition of carbon[7, 16] or the pyrolysis of organic thin films.[17] The work described herein takes a slightly different tactic by preparing C-OTEs via the pyrolysis of thin films of photoresist. We show that this approach, which

extends advances recently detailed by other laboratories for the preparation of much thicker (i.e., nontransparent) carbon film electrodes,[18-21] yields mechanically robust, amorphous carbon coatings that are optically transparent at thicknesses less than ~80 nm. Herein, we detail the findings from characterizations of the transmittance, electrical resistivity, surface composition, and topographic roughness of this new form of C-OTE, along with preliminary applications in both conventional and single molecule spectroelectrochemistry. The latter application represents, to our knowledge, the first example of the union of electrochemistry and single molecule spectroscopy.

2. Experimental

C-OTE Fabrication. The procedure for the fabrication of our C-OTEs consists of five steps. It represents a minor modification of the procedure detailed by the Kinoshita[19] and McCreery laboratories[20] for the preparation of much thicker (i.e., nontransparent) carbon electrodes via the pyrolysis of photoresist films. The major difference is that the starting material was diluted with its solvent to decrease its viscosity to allow the casting of a thinner film. In Step 1, quartz slides (Technical Glass) are rinsed rigorously with acetone and isopropanol, and dried under a stream of high purity nitrogen.

In Step 2, the positive photoresist AZ P4330-RS (Clarian) is diluted with 1-methoxy-2-propanol acetate to 25-50% (v/v) of the as-received material. Dilution reduces the viscosity of the resist solution to levels needed to cast films sufficiently thin to exhibit optical transparency after pyrolysis. Step 3 spin coats the diluted photoresist at 6000 rpm for 30 s onto a quartz substrate, and Step 4 "soft bakes" the coated substrate at 110°C for 60 s in a muffle furnace.

In Step 5, the sample is pyrolyzed in a furnace (Lindberg Blue M model 54253) that is fitted with a hard-fired alumina tube. This step begins by flushing the system at 1000 sccm with forming gas (95:5% nitrogen:hydrogen (v/v)) for 5 min, temporarily pumping the system down to 200 mTorr, and flowing the forming gas through the system for an additional 10 min. Next, the sample is pyrolyzed by ramping the temperature to 1000°C at 10°C/min. The temperature is held at 1000°C for 1 h while continuously flowing the forming gas at 1000 sccm through the alumina tube. The system is then allowed to radiatively cool to room temperature while maintaining the flow of forming gas. After terminating the flow of forming gas, the alumina tube is backfilled with high purity nitrogen.

Samples were stored before use in a glass microscope slide carrier for a minimum of three days, which reflects earlier observations that the spontaneous surface oxidation of much thicker pyrolyzed films of the photoresist levels off after three days of air-exposure.[22] The electrodes adhered strongly to the substrate. For example, extended sonication in various solvents had no effect on the surface. Moreover, the surface is mechanically rugged, requiring a sharp stylus to leave striations. However, the material does occasionally delaminate after extensive application of an applied potential at the limits of the working potential window (i.e., values of E_{app} less than -1.0 V or greater than E_{app} > +1.0 V).

Material Characterizations. Sheet resistance measurements were performed with a Keithley 2400 Source Meter that was connected through a breakout box to a probe card mounted on a microscope. This setup provided the capability of performing four-point probe determinations of sheet resistance. The voltage drop was measured at four or more different locations on each sample to determine the average film resistivity and its lateral variation.

Film thicknesses were assessed with a surface profilometer (Dektak IIA, Sloan), using samples photolithographically patterned to expose the underlying substrate prior to pyrolysis. The procedure first soft-baked the resist for 60 s at 110 °C. The next step used a positive transparency mask with varied sized features (50, 100, and 350 µm) for the localized patterning and exposure of the samples to a UV flood source. The resist was then immersed in a 1:5 (v:v) dilution of AZ 400K developer in water for 45 s, dried under a stream of high purity nitrogen, and imaged by AFM. There was no visible or microscopic evidence that the development step etched the underlying quartz substrate.

The surface roughness of the films were assessed using a NanoScope III atomic force microscope (AFM, Digital instruments) with silicon TESP probe tips (Nanosensors). All absorbance measurements were carried out with an HP 8453 UV-VIS spectrometer, and were corrected for contributions from the supporting quartz substrate.

Electrochemical experiments employed a Bipotentiostat Model AFCBP1 (Pine), a silver/silver chloride (Ag/AgCl, saturated KCl) reference electrode, and a platinum wire as the counter electrode. Ferrocyanide (Aldrich) and hydroxymethylferrocene (Aldrich) were used as test redox couples, which both have approximate formal reduction potentials of +0.225 V (vs. Ag/AgCl, saturated KCl) in 1.0 M potassium chloride (Aldrich). These experiments were performed without iR compensation.

Spectroelectrochemistry. Conventional spectroelectrochemical studies used a cell based on the classic design of Kuwana and co-workers[1] in which the probe beam is oriented normal to the electrode surface. A 0.6-cm diameter O-ring, which sealed the electrode to the cell, defined the geometric area of the electrode (0.28 cm^2) exposed to solution. Electrical contact to the C-OTEs was made with adhesive copper tape, cut to have a circular opening

slightly larger than the O-ring. The analyte was 10.0 mM ferrocyanide in 1.0 M potassium chloride (KCl). In these experiments, performed in chronoabsoptometry mode, the absorption at 420 nm was used to follow the formation of ferricyanide when the applied potential was changed from 0.00 to +0.60 V.

The instrumental setup for the evanescent-wave excitation geometry used for single molecule spectroelectrochemistry is partially shown in Figure 1a.[24] A detailed view of the spectroelectrochemical cell is given in Figure 1b. The setup entails the addition of 20 μL of 50 pM YOYO-I-labeled λ-DNA in 10 mM Gly-Gly buffer (pH 8.2) into a reservoir defined by a molded housing fashioned from a 150-μm thick block of polydimethylsiloxane (PDMS), a No. 1 (170-μm thick) Corning glass coverslip, and a 35-nm thick C-OTE. A DC power supply (Array Electronic) and a two-electrode system were used. A platinum wire served as the counter electrode, while the positive lead of the power supply was connected to the C-OTE with adhesive copper tape. The assembly was placed on the prism with index-matching oil to achieve airless contact. A laser beam was focused and directed through the prism at an angle of incidence of ~66° with respect to the quartz slide-sample interface. The laser beam was totally internally reflected at the C-OTE/solution interface, creating an evanescent field with a penetration depth of 110-120 nm. Fluorescent molecules within this field can therefore be excited and imaged.

An argon ion laser (Innova-90, Coherent) was operated at 488 nm as the excitation source. Extraneous light and plasma lines from the laser were removed by an equilateral prism and a pinhole placed prior to the entrance to the observation region. The total laser power, prior the prism, was ~10 mW. The microscope objective was a Zeiss 40× Plan-Neofluar (oil 1.3 NA). The objective was coupled to the coverslip with immersion oil (type

FF, n = 1.48, Cargill). Images of the irradiated region were recorded with an intensified CCD camera (Cascade, Roper Scientific). The camera was held at $-35°$ C.

A 488-nm holographic notch filter (Kaiser Optical) with an optical density >6 was placed between the objective and CCD camera. The digitization rate of the CCD camera was 1 MHz (16 bits). The digital-analog converter setting was 3689. The frame-transfer function of the CCD camera was operated in the external synchronization mode, with the exposure timing for the camera and laser shutter synchronized by a shutter driver/timer (Uniblitz ST132, Vincent Associates). The CCD exposure frequency was 1 Hz. The exposure time for each frame was 10 ms. A sequence of frames were acquired in each experiment via V^{++} software (Roper Scientific).

λ-DNA (48502 bp, fully extended length of ~16 μm, Life Technologies) samples were prepared in 10 mM Gly-Gly buffer at pH 8.2. The DNA samples were labeled using a ratio of one YOYO-I (Molecular Probes) dye molecule per five base pairs. The Gly-Gly buffer solutions were previously photobleached under a mercury lamp for ~12 h and passed through a 0.2-μm filter. Quantification was achieved using counting software.

3. Results and Discussion

Material Characterization. The results from several characterizations of the material properties (i.e., thickness, roughness, transmittance, and sheet resistance) of our C-OTEs are presented in Table 1 and Figures 2-4. The results and discussion from X-ray photoelectron and Raman spectroscopy studies are provided as Supporting Information.

Film thicknesses. Table 1 summarizes the dependence of the pyrolyzed film thickness as a function of photoresist concentration and number of coatings. As expected, the pyrolyzed

film thickness increases with photoresist concentration and the number of coating depositions. A coating cast once from a 50% dilution, for example, yields a thickness of 70 $\pm$ 0.4 nm, whereas that from a 25% dilution is 13 $\pm$ 0.7 nm. The number of depositions prior to pyrolysis can also be used to manipulate the film thickness. Multiple depositions of the photoresist lead to small, but readily detectable increases in thickness (3 to 7 nm). Comparison of pre-and post-pyrolysis film thicknesses indicates that pyrolysis causes a 75-80% decrease in film thickness.

Optical Transparency. Figure 2 displays the optical transmittance from 300 to 700 nm for quartz slides coated with three different thicknesses of pyrolyzed carbon: 13, 35, and 79 nm. The spectra show that: 1) transmittance increases as the thickness of the coating decreases; and 2) transmittance at a given coating thickness increases as wavelength increases. That is, the 13-nm film has a 33% transmittance at a wavelength of 300 nm, whereas that for the 79-nm film is 1%.

In contrast, the transmittance at a wavelength of 700 nm for the 13-nm film reaches 53%, and that for the 79-nm film is 15%. These results are consistent with expectations from the wavelength dependencies of carrier absorption and film thickness.[25-28] The transmittance of our C-OTEs is in the same range of other metallic OTEs but is slightly less than that of OTEs like indium tin oxide.[4, 6]

Electrical Conduction. The electrical characteristics of our C-OTEs as a function of film thickness were evaluated via sheet resistance (R_s) measurements with an in-house constructed four-point probe. These results are presented in Figure 3 for pyrolyzed film thicknesses up to ~500 nm. As is evident, R_s undergoes a slow increase as the film thickness decreases from ~500 nm to ~35 nm. Below ~35 nm, however, R_s exhibits a more dramatic

increase as thickness decreases. This dependence mimics that for sputter-deposited carbon films,[16] as well as that for ultrathin metal and semiconductor films.[5, 29] The basis for the evolution of the electrical properties of our films is briefly examined below.

Lastly, by incorporating the film thickness into the sheet resistance measurements, the resistivity can be calculated. The average resistivity for C-OTEs that are 35 to 80 nm thick is 2.4×10^{-3} Ω-cm with a standard deviation of 3.1×10^{-4}, assuming the sheet resistance over these thicknesses follows a linear dependence. This value compares well with the resistivity reported for thick, non-transparent films of pyrolyzed photoresist (5.7×10^{-3} Ω-cm).[20, 21]

Material Composition. The elemental composition of the C-OTEs was evaluated via XPS and closely matched that found for the much thicker versions of this material.[20]

The Raman spectroscopy analysis revealed that the microcrystalline structure of the C-OTEs is also similar to thick film PPF. A detailed discussion of both sets of data is available as Supporting Information.

Surface Roughness. The surface topography of our C-OTEs was evaluated by tapping mode atomic force microscopy (AFM). Images (40 x 40 μm) are presented in Figure 4 for C-OTEs with thickness of 18 and 55 nm, along with an image of an uncoated quartz substrate for comparative purposes. Cross-sectional plots accompany each image. The images show that the underlying substrate is much rougher than the two carbon-coated samples. The quartz substrate has a large number of spike-like features that extend slightly beyond the scale of the z-axis of the image. Based on images from several different quartz substrates, the root-mean-square (RMS) roughness of these quartz substrates is ~2.6 nm.

The presence of the spikes diminishes upon the formation of the pyrolyzed film. This decrease is attributed to the conformal behavior of the photoresist during deposition and/or

the melting of the coating in the early stages of heat treatment. As a consequence, the RMS roughness of the 18-nm coating is 0.8 nm and that for the 55-nm coating is 0.5 nm. The latter coating therefore exhibits a smoothness that rivals those found at gold films that are prepared by extended annealing and templating procedures.[30-32] These images also show the occasional presence of larger imperfections in the underlying substrate, which we attribute to striations from the final stages of polishing by the manufacturer.

The smoothness of these C-OTEs points to an intriguing explanation for the transition observed in the sheet resistance data in Figure 3. In the growth of thin metal and semiconductor films, the coating forms first as discontinuous islands that eventually coalesce as thickness increases. The resistance of these materials therefore evolves via a percolation model due to the diffuse scattering of carriers at the air-metal and metal-substrate interfaces.[5, 29] The AFM images in Figure 4, however, suggest that the pyrolyzed carbon films form a continuous coating even at exceedingly low thicknesses (e.g.10 nm); there is little evidence for defects or pin holes as would be expected with the island growth process of metallic thin films.[16, 28] Interestingly, evaporated carbon films with a continuous structure have been reported for thicknesses as low as 2 nm when formed on the atomically smooth terraces of single crystals.[33] In these cases, the decrease in conductivity associated with decreasing film thickness is attributed to a progressive restriction of hopping conductivity,[28, 33-35] a mechanism that may also be operative on our C-OTEs.

Electrochemical Performance. Figure 5 presents steady-state cyclic voltammograms (1 mV/s) for 1.0 mM solutions of hydroxymethylferrocene (HMF) and 1.0 mM ferrocyanide, both in 1.0 M KCl. These curves were collected using a 35-nm C-OTE as the working electrode. The peak separation for HMF/HMF$^+$, a kinetically fast redox couple, is close to the

reversible value of 60 mV. That for $Fe(CN)_6^{3-/4-}$, which is a slower couple and more sensitive to surface interactions, is much larger at 95 mV.[15, 22, 37] Scans at higher sweep rates for both systems, however, exhibit much larger peak separations as a consequence in large part of the internal resistance of the exceedingly thin electrode material.[38]

Figure 5 also presents a scan at 1 mV/s in only supporting electrolyte (1.0 M KCl). The response indicates that our C-OTEs have a large accessible potential window, enabling electrochemical investigation at large anodic and cathodic potentials. The curve also shows a low level of oxygen reduction at –0.4 V.[19] The working potential window of 2 V is similar to that of indium-tin oxide electrodes.[4] It also surpasses that typically accessible with glassy carbon, but is a little less than that for doped diamond films.[39] The scan in 1.0 M KCl can also be used to determine the capacitance of the C-OTE/supporting electrolyte interface. This analysis yields a value of 6.5 $\mu F/cm^2$, which is on par with values reported for thick film electrodes of pyrolyzed photoresist[22] and diamond electrodes.[39]

Spectroelectrochemical Performance. The potential utility of our C-OTEs to follow a change in the spectral characteristics of a redox couple with respect to a change in applied potential was carried out using chronoabsorptometry. This experiment employed an SEC cell of conventional design, 10.0 mM ferrocyanide in 1.0 M KCl as the chromophoric redox probe, a 35-nm thick C-OTE, and a potential step from 0.00 to +0.60 V. Figure 6 presents the evolution of the spectral response between 370 and 480 nm, and shows an increase in absorbance with time, which is consistent with the generation of ferricyanide ($\lambda_{max} = 420$ nm; $\varepsilon_{max} = 1020$ M^{-1}-cm^{-1}).[40] A linear relationship (correlation coefficient of 0.998) between the change in absorbance (ΔA) and the square root of time ($t^{1/2}$) confirms the effective performance of this material for use in a traditional spectroelectrochemical format (i.e. semi-

infinite linear diffusion conditions prevail). The equation for the resulting linear plot is $\Delta A =$ $-0.014\,t^{1/2} + 0.068$.

Single Molecule Monitoring at Electrified C-OTEs. To probe the potential utility of our C-OTEs as substrates for investigations by single molecule spectroscopy, the ability to monitor the potential dependence of the adsorption of YOYO-I labeled λ-DNA was investigated. Since the rate of diffusion for small molecules in water is large, residence times in the evanescent field layer (EFL) are fairly short. Small molecules, as a consequence, appear in the EFL for only one frame at frame rates less than 10 Hz when freely diffusing and not attractively interacting with the surface.[41] It is therefore challenging to track freely diffusing, small molecules from one frame to the next. Much larger biomolecules, like λ-DNA with unpaired bases at the ends that can interact with the surface, however, reside longer within the thin EFL and can be continuously monitored for several consecutive frames, and for an even longer period of time when adsorbed.[24, 42] This situation provides a basis for a preliminary assessment of the ability to track the adsorption of individual YOYO-I labeled λ-DNA at the electrified interface of a C-OTE.

An example of the results from these proof-of-concept tests are presented in the 60 x 80 μm images in Figure 7 (movie 7 in Supporting Information). Figure 7A is an image at the C-OTE/electrolyte interface prior to application of a +1.5 V potential difference between the C-OTE and platinum counter electrode. Each bright spot represents one single tagged λ-DNA molecule in the EFL. In general, most of the molecules are freely diffusing, appearing and disappearing at random locations on successive image frames upon movement into and out of the EFL. Very few (if any) can be tracked from one frame to the next.

After the application of +1.5 V to the C-OTE, the number of λ-DNA observed in the EFL begins to increase. This increase is evident upon examination of Figures 7B, C, which were obtained 10 and 60 s after voltage application, respectively. The evolution of the images is attributed to the gradual increase in the positive surface charge density of the carbon film, which would result in an increase in the electrostatic attraction with the high, negative charge density of DNA at pH 8.2.[43]

The evolution of these images yields another interesting point. While the apparent number of molecules in the EFL clearly increases, there is little evidence for an increase in residence time for DNA molecules. They are not attached to the surface but freely moving under these low potentials. When the C-OTE is grounded after the +1.5 V experiment, the number of λ-DNA molecules observed is similar to that prior to application of any potential (as in Figure 7A). This result differs from our earlier reports in which λ-DNA, when adsorbed on the surface of thiol-derived monolayers on gold with different terminal groups or on that of a metal oxide, remained fixed on the same location at the surface for a large number (tens to hundreds) of consecutive image frames.[42, 43] Studies in which the effect of applied potential and pH, the latter of which can be used to manipulate the charge density on the DNA backbone, are necessary before we can speculate much further as to the basis of this difference.

Further evidence for the potential dependence of adsorption by single molecule spectroelectrochemistry is presented by the plot in Figure 8. This plot summarizes the number of λ-DNA detectably present in the EFL as a function of time for potential differences of +1.0 and +1.5 V. The plot for +1.5 V shows an increase in the number of observed molecules from an initial level of just under 50 to over 400 within the time course

of the experiment. Importantly, the plot at +1.0 V is notably different in that the increase is markedly smaller. These contrasting results are qualitatively consistent with the expectation of a larger electrostatic attraction of λ-DNA to the carbon electrode at the more positive value of the potential differences.

In completing this first study, we also examined the effect of a much larger value of potential difference, +5.0 V. The images obtained in this experiment (data not shown) yielded a much greater number of molecules present in the EFL, with a large fraction strongly adsorbed for a number (tens to hundreds) of consecutive image frames. This result is attributed to the oxidation of the C-OTE surface, which then appears to adsorb λ-DNA at a magnitude more like that found at the two types of surfaces used in our earlier reports.[42] Moreover, the oxidation appeared irreversible because grounding the C-OTE had little effect on the strongly adsorbed λ-DNA molecules.

4. Conclusions

In conclusion, dilute solutions of photoresist serve as an excellent starting material for the manufacture of C-OTEs. The thickness of the PPFs can easily be adjusted to fit different applications. Optical transparency is achieved for C-OTEs with a thickness of less than ~80 nm while conductivity is sufficient for films that are thicker than 35 nm. Cleaning is achieved easily without damaging the electrodes. Overall, the C-OTE composition, smoothness, and performance are comparable to thick pyrolyzed photoresist films already utilized by the research community. The mechanical stability, transparency and conductivity make this form of C-OTEs an interesting alternative to existing OTEs. Efforts to exploit the utility of this

system to probe the effect of applied potential by single molecule spectroelectrochemistry are underway. Studies of adsorption at modified carbon electrodes are also planned.

5. Acknowledgements

6. Supporting Information

More detailed information on the XPS and Raman analysis is available. AVI movie as noted in the text, and represents a continuous 60-s observation window compressed to 20 s. This material is available free of charge as Supporting Information via the Internet at http://pubs.acs.org/ac.

7. References

(1)   Kuwana, T.; Winograd, N. In *Electroanalytical Chemistry*; Bard, A. J., Ed.; Marcel Dekker, Inc.: New York, 1974; Vol. 7, pp 1-78.

(2)   Heineman, W. R.; Hawkridge, F. M.; Blount, H. N. *Journal of Electroanalytical Chemistry* **1984**, *13*, 1-113.

(3)   Stotter, J.; Haymond, S.; Zak, J. K.; Show, Y.; Cvackova, Z.; Swain, G. M. *Electrochemical Society Interface* **2003**, *12*, 33-38.

(4)   Zudans, I.; Paddock, J. R.; Kuramitz, H.; Maghasi, A. T.; Wansapura, C. M.; Conklin, S. D.; Kaval, N.; Shtoyko, T.; Monk, D. J.; Bryan, S. A.; Hubler, T. L.; Richardson, J. N.; Seliskar, C. J.; Heineman, W. R. *Journal of Electroanalytical Chemistry* **2004**, *565*, 311-320.

(5)   Mattson, J. S.; Smith, C. A. *Analytical Chemistry* **1975**, *47*, 1122-1125.

(6)   Haacke, G. *Annual Review of Material Science* **1977**, *7*, 73-93.

(7)   DeAngelis, T. P.; Hurst, R. W.; Yacynych, A. M.; Mark, H. B.; Heineman, W. R.; Mattson, J. S. *Analytical Chemistry* **1977**, *49*, 1395-1398.

(8)   Haymond, S.; Zak, J. K.; Show, Y.; Butler, J. E.; Babcock, G. T.; Swain, G. M. *Analytical Chimica Acta* **2003**, *500*, 137-144.

(9)   Petek, M.; Neal, T. E.; Murray, R. W. *Analytical Chemistry* **1971**, *43*, 1069-1074.

(10)   Hong, H.; Porter, M. D. *Journal of Electroanalytical Chemistry* **2005**, *578*, 113-119.

(11)   Harnisch, J. A.; Porter, M. D. *Analyst* **2001**, *126*, 1841-1849.

(12)   Ponton, L.; Porter, M. D. *Analytical Chemistry* **2004**, *76*, 5823-5828.

(13)   Keller, D. W.; Porter, M. D. *Analytical Chemistry* **2005**, *77*, 7399-7407.

(14)   Randin, J. P.; Yeager, E. *Electroanalytical Chemistry and Interfacial Electrochemistry* **1975**, *58*, 313-322.

(15)   McCreery, R. L. In *Interfacial Electrochemistry*; Wieckowski, A., Ed.; Marcel Dekker, Inc.: New York, 1999, pp 631-647.

(16)   Dawson, J. C.; Adkins, C. J. *Journal of Physics: Condensed Matter* **1995**, *7*, 6297-6315.

(17)   Anjo, D. M.; Brown, S.; Wang, W. *Analytical Chemistry* **1993**, *65*, 317-319.

(18)   Lyons, A. M. *Journal of Non-Crystaline Solids* **1985**, *70*, 99-109.

(19)   Kim, J.; Song, X.; Kinoshita, K.; Madou, M.; White, R. *Journal of the Electrochemical Society* **1998**, *145*, 2314-2319.

(20)   Ranganathan, S.; McCreery, R. L.; Majji, S. M.; Madou, M. *Journal of The Electrochemical Society* **2000**, *147*, 277-282.

(21)   Kostecki, R.; Schnyder, B.; Alliata, D.; Song, X.; Kinoshita, K.; Koetz, R. *Thin Solid Films* **2001**, *396*, 36-43.

(22)   Ranganathan, S.; McCreery, R. L. *Analytical Chemistry* **2001**, *73*, 893.

(23)   Kang, S. H.; Shortreed, M. R.; Yeung, E. S. *Analytical Chemistry* **2001**, *73*, 1091-1099.

(24)   Williams, M. W.; Arakawa, E. T. *Journal of Applied Physics* **1972**, *43*, 3460-3463.

(25)   Taft, E. A.; Philipp, H. R. *Physical Review* **1965**, *138*, A197-A202.

(26)   Greenaway, D. L.; Harbeke, G. *Physical Review* **1969**, *178*, 1340-1348.

(27)   Adkins, C. J.; Hamilton, E. M., Eliat, Israel 1971; Taylor & Francis Ltd.; 229-233.

(28)   Levchenko, I.; Baranov, O. *Vacuum* **2004**, *72*, 205-210.

(29)   Hegner, M.; Wagner, P.; Semenza, G. *Surface Science* **1993**, *291*, 39-46.

(30)   Wagner, P.; Hegner, M.; Guentherodt, H. J.; Semenza, G. *Langmuir* **1995**, *11*, 3867-3875.

(31)   Wong, S. S.; Porter, M. D. *Journal of the Electrochemical Society* **2000**, *485*, 135-143.

(32)   MacVicar, M. L. A. *Journal of Applied Physics* **1970**, *41*, 4765-4768.

(33)   McLintock, I. S.; Orr, J. C. In *Chemistry and Physics of Carbon*; Walker, P. L., Thrower, P. A., Eds.; Marcel Dekker: New York, 1973; Vol. 11, pp 243-312.

(34)   Morgan, M. *Thin Solid Films* **1971**, *7*, 313-323.

(35)   Shporer, M.; Ron, G.; Loewenstein, A.; Navon, G. *Inorganic Chemistry* **1965**, *4*, 361-364.

(36)   Based on the 35 nm electrode thickness and 0.3 cm working electrode radius, an internal resistance of ~6.1 kOhm was measured.

(37)   Witek, M.; Wang, J.; Stotter, J.; Hupert, M.; Haymond; Sonthalia, P.; Swain, G. M. *Journal of Wide Bandgap Materials* **2001**, *8*, 171-788.

(38)   Porter, M. D.; Kuwana, T. *Analytical Chemistry* **1984**, *56*, 529-534.

(39)   He, Y.; Li, H. W.; Yeung, E. S. *Journal of Physical Chemistry B* **2005**, *109*, 8820-8832.

(40)   Li, H. W.; Park, H. Y.; Porter, M. D.; Yeung, E. S. *Analytical Chemistry* **2005**, *77*, 3256-3260.

(41)   Since the actual electrode potential is unknown, the evolution of the images may also arise from a decrease in the negative charge density of the carbon electrode, depending on the location of the potential of zero charge with respect to the applied bias voltage.

8. Tables

Table 1. Thickness of C-OTEs as a function of AZ 4330 concentration and number of depositions.

AZ 4330 Concentration (%V)	Number of Coatings[a]	PPF Thickness (nm)[b]
50	1	70 ± 0.4
	2	77 ± 3.3
33	1	35 ± 0.6
	2	39 ± 3.3
25	1	13 ± 0.7
	2	19 ± 1.4
	3	23 ± 2.0
	4	26 ± 2.5

[a]Each subsequent coating was deposited after allowing the previous coating to air-dry for 30 min. [b]Film thicknesses were determined by profilometry for samples that were photolithographically patterned before pyrolysis. The uncertainties represent the average thickness variation for three measurements on three different samples.

9. Figures
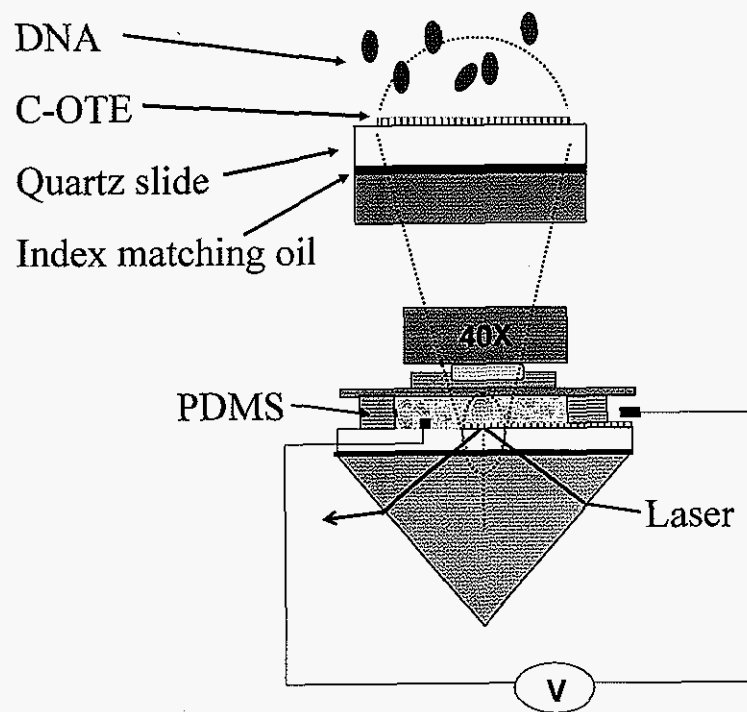
Figure 1a. Side view of Single Molecule Spectroscopy setup (partial) with expanded view of the detection region.
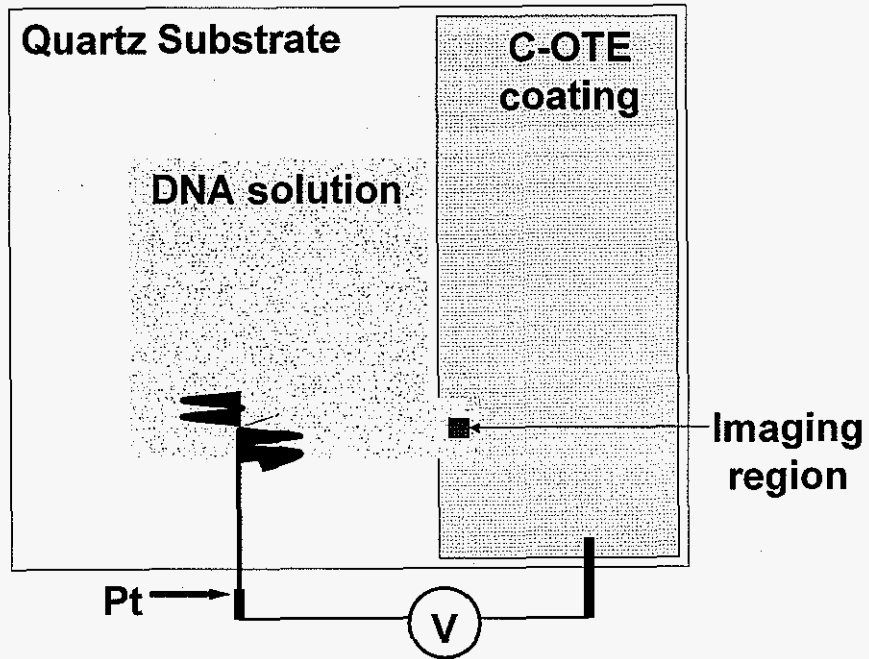
Figure 1b. Top view of electrochemical cell. PDMS confining the DNA solution and the glass cover slide are not shown.
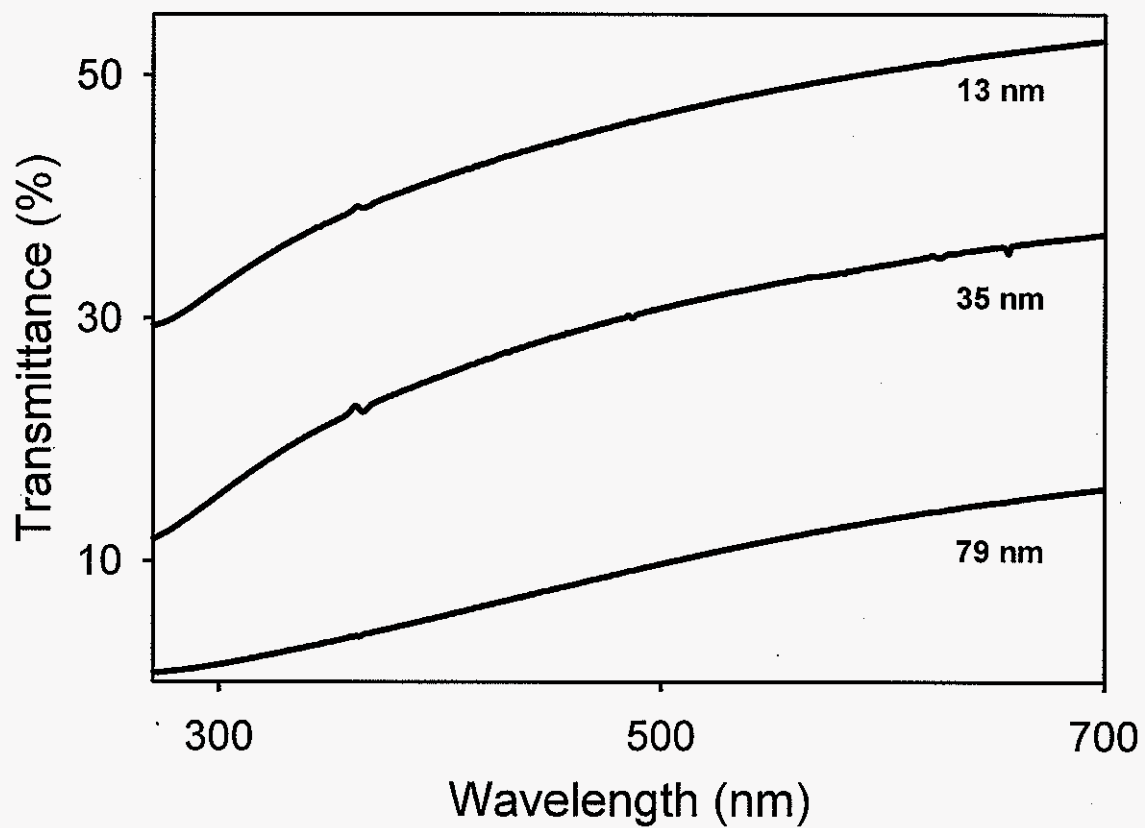
Figure 2. Optical transmittance of C-OTEs as a function of wavelength for three different pyrolyzed film thicknesses (13, 35, and 79 nm).
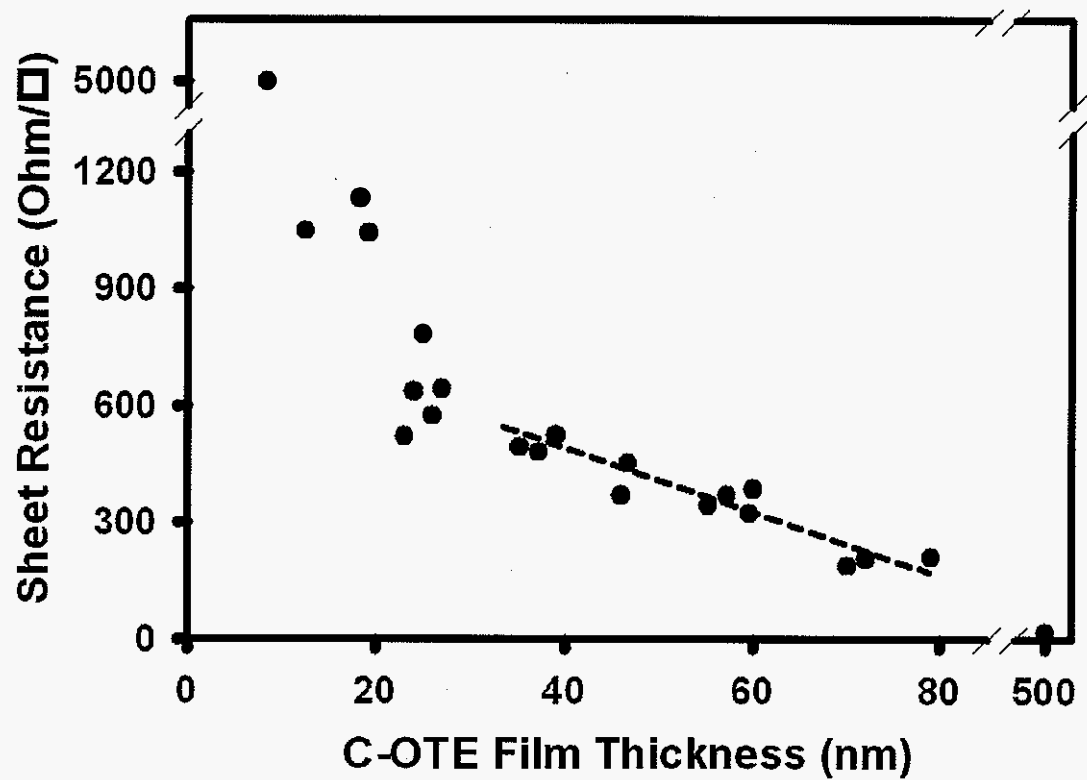
Figure 3. Sheet resistance of C-OTE as a function of pyrolyzed film thickness. The equation for the linear fit to the dependence of the sheet resistance (R_s) and pyrolyzed film thickness (d) between 35 and 80 nm is $R_s = -7.6d + 776$.
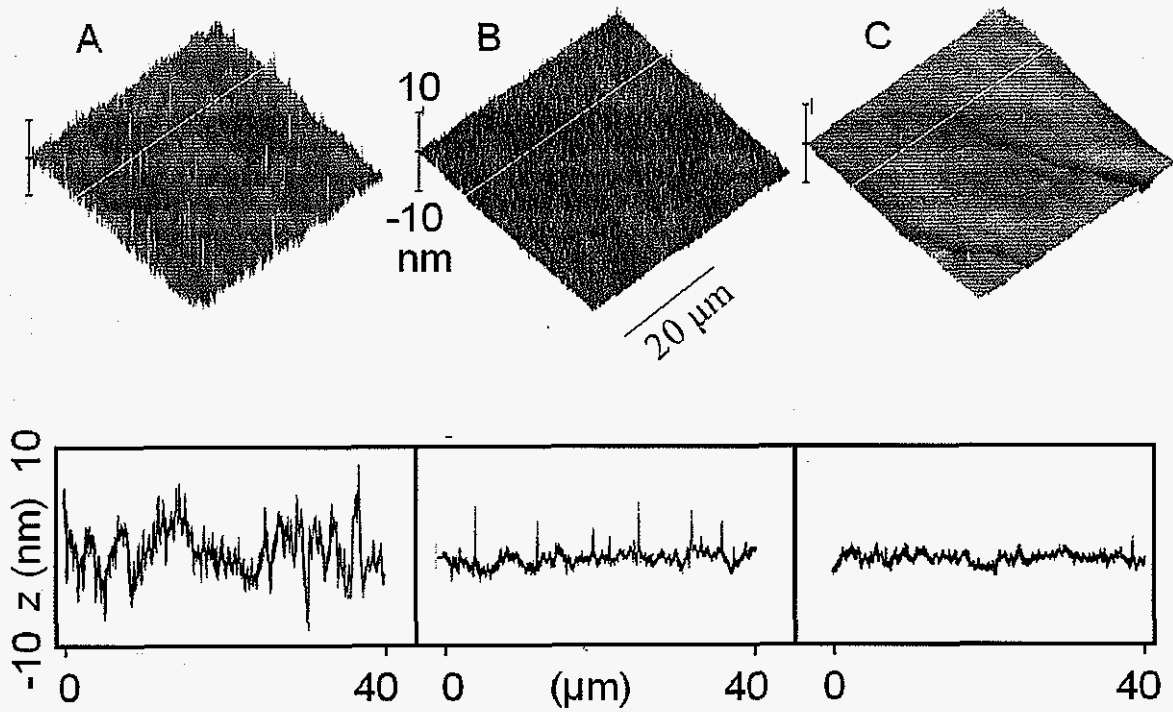
Figure 4. AFM images (40 x 40 μm) and cross-sectional plots of an uncoated quartz substrate (A) and C-OTEs with thicknesses of 18 nm (B) and 55 nm (C).
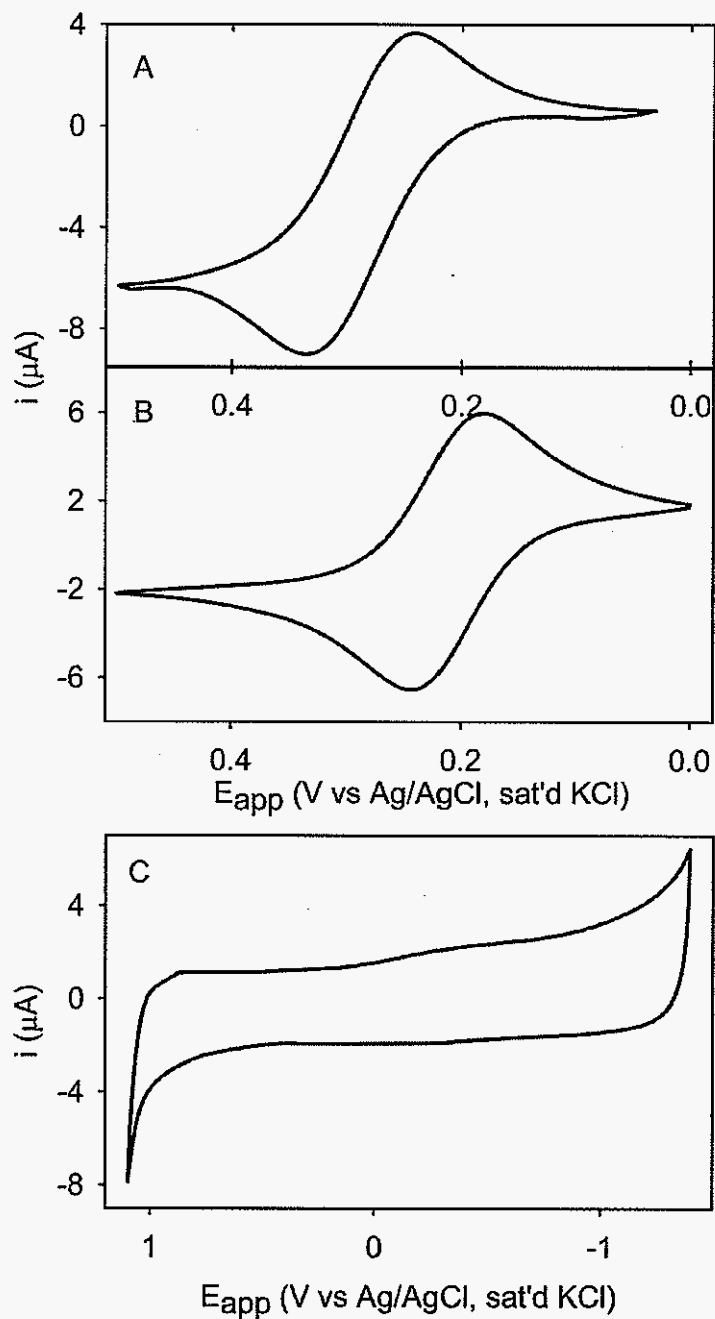
Figure 5. Steady-state cyclic voltammetric responses of a 35 nm C-OTE in A) 1.0 mM ferrocyanide, B) 1.0 mM hydroxymethylferrocene, and C) supporting electrolyte. In all cases, the supporting electrolyte was 1.0 M KCl. RE = Ag/AgCl in sat. KCl, CE = Pt wire, geometric electrode area A = 0.28 cm^2. Scan rate = 1 mV/s.
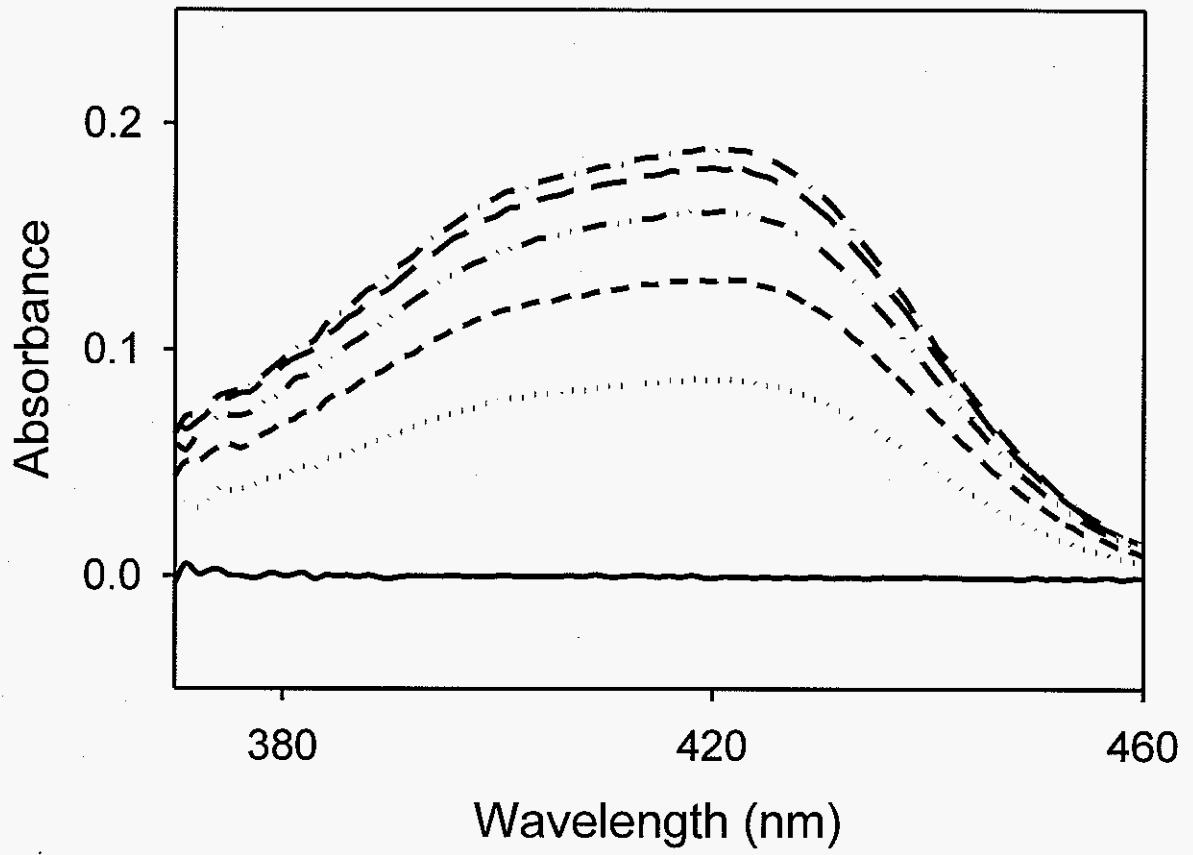
Figure 6. Chronoabsorptometry results for the oxidation of ferrocyanide upon the change in applied potential from 0.00 to +0.60 V on a 35 nm C-OTE.
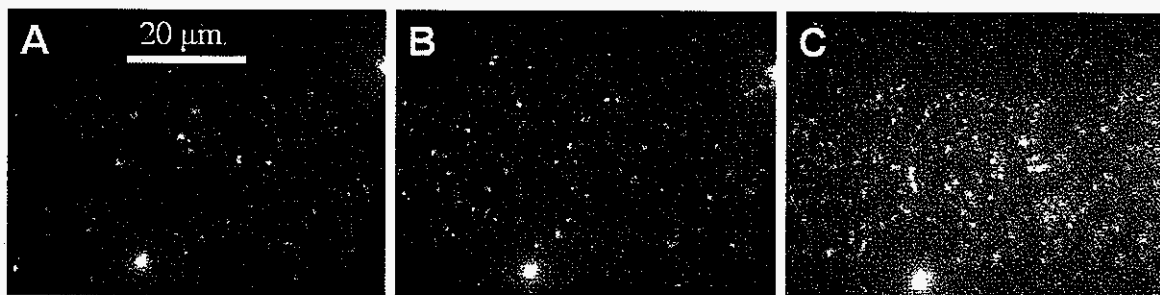
Figure 7. Fluorescent images of YOYO-I labeled λ-DNA at the C-OTE/aqueous interface: (A) prior to the application of a potential difference between the C-OTE and a platinum counter electrode; (B) and (C) 10 and 60 s after application of +1.5 V to the C-OTE. Note that (A) corresponds to 0.45-s into the movie, and that (B) and (C) reflect images at 2.89 and 19.97 s into the movie respectively. The image dimensions are 60 x 80 μm, C-OTE thickness is 35 nm, and the λ-DNA concentration is 50 pM in 10 mM Gly-Gly buffer (pH 8.2).
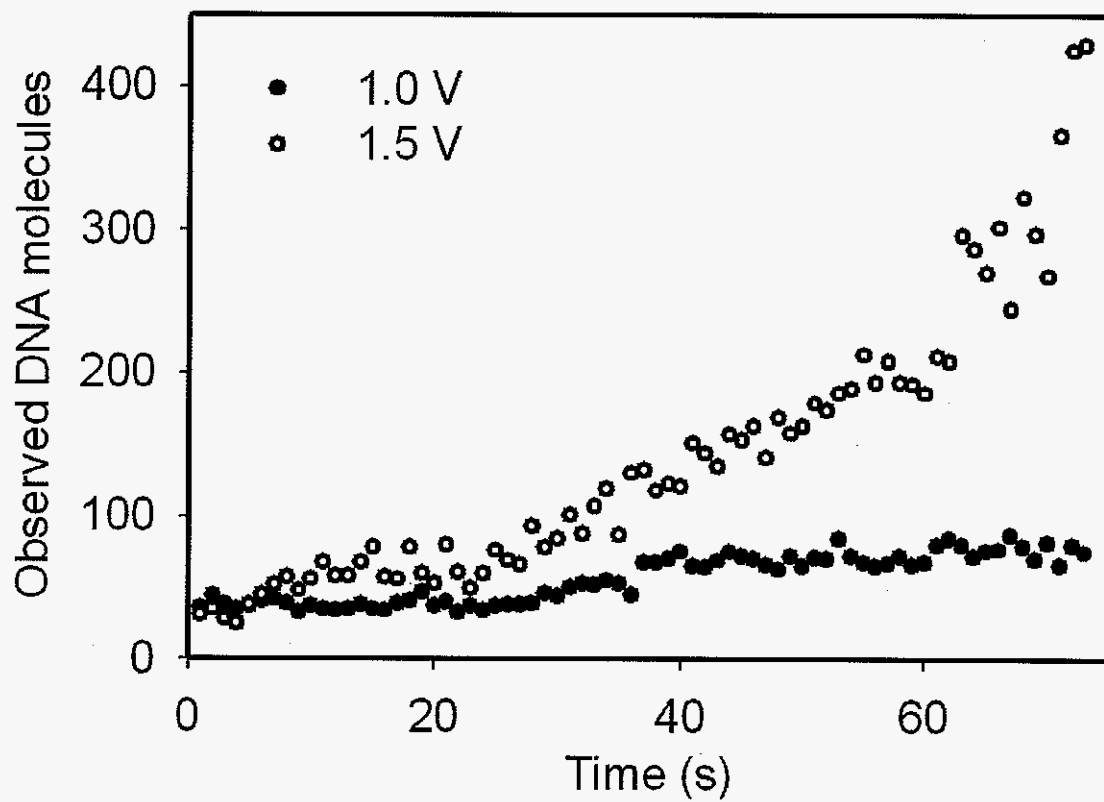
Figure 8. Time dependence of DNA molecules appearing within the evanescent field layer upon applying a potential of 1.0 V and 1.5 V.

10. Supplemental Supporting Information

Abstract

This supporting information section describes the X-ray photoelectron (XPS) and Raman spectroscopy analysis for the C-OTEs presented in the above-mentioned article. Our results agree well with the XPS and Raman analysis performed by others on thick-film pyrolyzed photoresist films.[1,2]

Discussion

XPS Analysis. The elemental composition of the electrode surfaces was characterized by XPS, using a Physical Electronics Industries 5500 Surface Analysis System. XPS survey spectra showed a predominance of carbon, as well as a low level of oxygen. Typical oxygen/carbon ratios were ~3%. These results were independent of pyrolyzed film thickness. Samples also contained trace levels of nitrogen and silicon, but were typically no more than 0.3 and 0.5% respectively.

Raman Spectroscopy. Raman spectroscopy was used to assess the graphitic nature of the pyrolyzed material. These measurements were preformed with a fiberoptic-based Raman system (NanoRaman I, Concurrent Analytical). The system is equipped with a CCD (Kodak 0401 E), which is electromechanically cooled to 0°C, and a Czerny-Turner imaging spectrometer (f/2.0). The HeNe laser (632.8 nm) power incident on the sample was 30 mW (390 μm^2 spot size). All spectra represent a 30-s integration time.

An assessment of the near-surface order of our nanometer-thick carbon revealed similarities with thick-film pyrolyzed photoresist. This analysis is based on a recent body of work that demonstrated the relative integrated intensities of the E_{2g} mode for sp^2 carbon and the so-called "D" band for vibrations associated with edge planes of a graphitic lattice qualitatively correlate with structural disorder.[1-3] In other words, the larger the D/E_{2g} ratio, the larger the edge plane density, and the smaller the average size of the graphitic crystallites.

The results of these characterizations are presented in Figure S1, which include spectra for 39 and 55 nm C-OTEs and GC-20 for comparison (GC-20 is the designation for glassy carbon (Tokai Carbon) that was prepared by heat treatment at 2000°C). The E_{2g} mode is assigned to the band at 1598 cm^{-1}, while that at 1329 cm^{-1} is attributed to the D band. The positions of these bands are consistent with use of a HeNe (632.8 nm) laser as the excitation source.[4] The D/E_{2g} ratio of integrated intensities for GC-20, obtained after spectral deconvolution, is 2.6. This value is in close agreement with that reported previously for GC-20,[4] which consists of very small graphitic crystallites. In contrast, the ratios for the 39 and 55-nm C-OTEs have slightly lower values, 2.3 and 2.4, respectively. The difference suggests that the structure of the C-OTEs is slightly more disordered than that of GC-20, an assertion supported by the broader nature of the bands for the C-OTEs relative to GC-20.

REFERENCES

(1)   Ranganathan, S.; McCreery, R. L. *Analytical Chemistry* **2001**, *73*, 893.
(2)   Kostecki, R.; Schnyder, B.; Alliata, D.; Song, X.; Kinoshita, K.; Koetz, R. *Thin Solid Films* **2001**, *396*, 36-43.
(3)   McCreery, R. L. In *Interfacial Electrochemistry*; Wieckowski, A., Ed.; Marcel Dekker, Inc.: New York, 1999, pp 631-647.
(4)   Wang, Y.; Alsmeyer, D. C.; McCreery, R. L. *Chemical Materials* **1990**, *2*, 557-563.
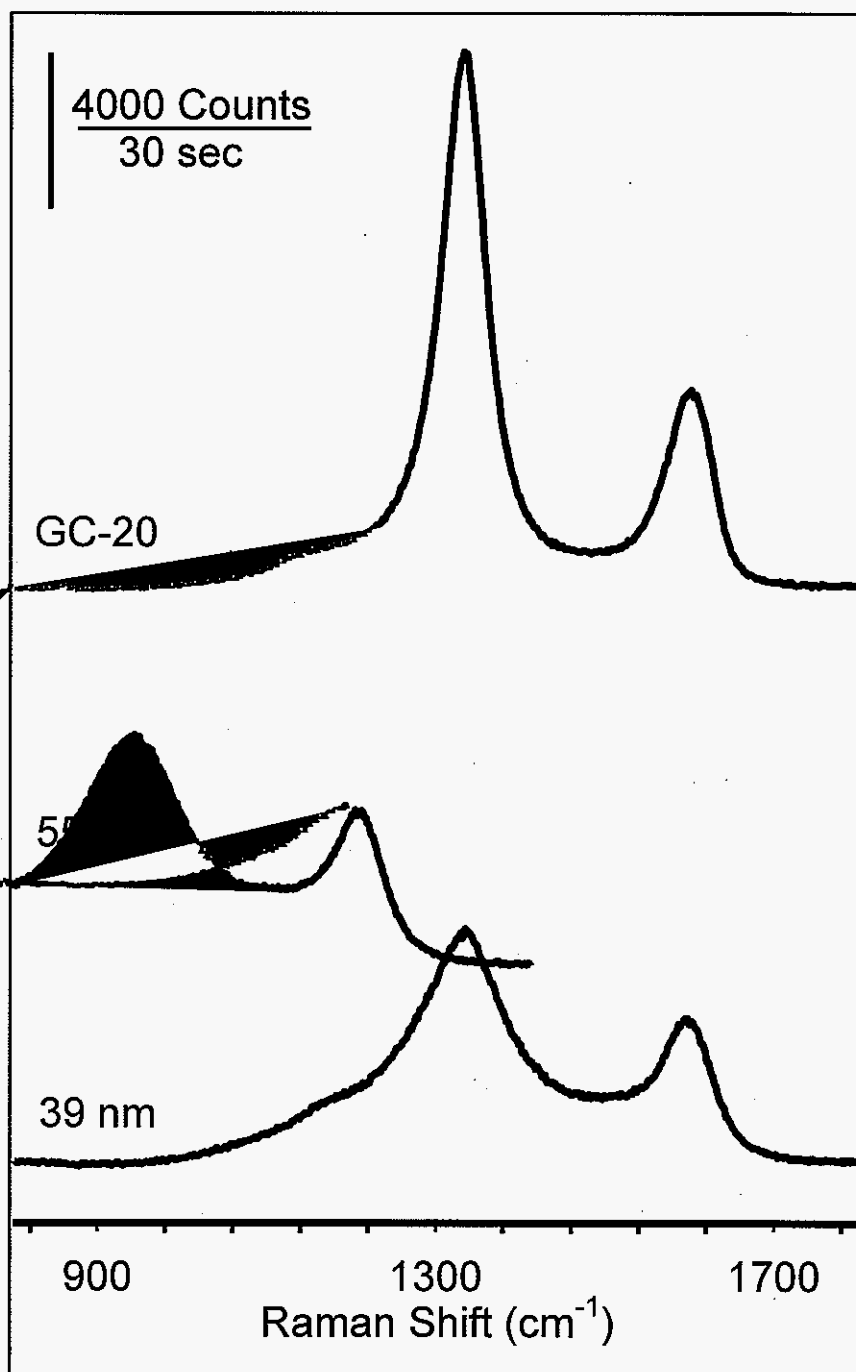
Figure S1. Raman analysis for glassy carbon (GC-20) and C-OTEs with 55 and 39 nm film thicknesses. Peak maxima at 1329 and 1598 cm^{-1}.

CHAPTER 3. SINGLE MOLECULE ADSORPTION AND DIFFUSION STUDY AT AN ELECTRIFIED CARBON INTERFACE USING SPECTROELECTROCHEMISTRY WITH CARBON-BASED OPTICALLY TRANSPARENT ELECTRODES

Sebastian Donner, Jiangwei Li, Edward S. Yeung, and Marc D. Porter[1]*

Ames Laboratory-U.S.D.O.E., Departments of Chemistry and of Chemical and Biological Engineering, and Institute for Combinatorial Discovery, Iowa State University, Ames, Iowa 50011

[1] Corresponding Author, Present Address: Department of Chemistry and of Chemical Engineering, University of Utah, Salt Lake City, UT 84112

Abstract

This paper describes the preparation and application of carbon-based optically transparent electrodes (C-OTEs) for investigations of the adsorption characteristics of single DNA molecules at electrified interfaces. Combining single molecule spectroscopy (SMS) with spectroelectrochemistry (SEC) enables interrogation of the movement and adsorption behavior of individual DNA molecules. We previously demonstrated this concept using λ-DNA and C-OTEs prepared with a positive photoresist as a precursor for the electrodes. For the present work, we developed C-OTEs prepared using negative photoresist SU 8-2000.5 as electrode starting material, and use three different sizes of DNA to study their adsorption and

diffusion behavior as individual molecules at an electrified carbon interface. Results point to surface defects as playing a key role in adsorption, along with an interesting transient response upon charges in applied potential due to contributions of the supporting electrolyte.

1. Introduction

Carbon is a widely used electrode material due to its wide potential window, low background current, and low cost.[1] In the past few years, our laboratory has been pursuing the development of electrochemically modulated liquid chromatography (EMLC), using stationary phases based on porous graphitic carbon or glassy carbon.[2] The use of a conductive stationary phase allows the controlled alteration of the surface charge density of the packing by changing the applied potential (E_{app}). This capability yields the ability to fine-tune analyte retention through E_{app}.

The application of carbon is extraordinarily widespread.[3-5] Yet events and transformations that occur on the single molecule level have been difficult to observe. While the carbon surface has been studied extensively, virtually all fundamental insights derive from the average response of a large ensemble of molecules. This situation is even further confounded being faced with a heterogeneous material such as carbon.

Past investigations of glassy carbon as packing material in EMLC have also revealed a difference in potential dependent adsorption for various surface sites.[6, 7] These results generally agreed with the findings from investigations of different types of carbon materials.[4] Studies on glassy carbon (GC) and highly oriented pyrolytic graphite (HOPG) with scanning tunneling microscopy (STM) further identified the importance of material structure, while also revealing the role of microscopic surface defects on the adsorption properties of carbon

electrodes.[8, 9]   The work herein attempts to build on such findings by furthering the development of optically transparent carbon electrodes (C-OTEs) and the coupling of this new material construct with single molecule spectroscopy (SMS).

Optically transparent electrodes (OTEs) are frequently used to measure chronophoric changes in redox couples over time and to investigate reaction mechanisms at electrified interfaces.[10-13]   Deposition of conductive thin films such as gold, platinum, indium and indium/tin oxide onto a suitably transparent substrate is a common method for OTE fabrication.[10-17]   The preparation of minigrid electrodes consisting of metallic microscreens[18] represents an alternative to thin film OTEs in an attempt to increase conductivity.

We recently reported on the fabrication of C-OTEs using the positive photoresist AZ 4330-RS as precursor.[19]   We also demonstrated their spectroelectrochemical applicability with SMS observations of the adsorption of YOYO labeled λ-DNA to the carbon electrode surface.   The influence of minute solvent evaporation prior to spin coating on the reproducibility of the thickness of the pyrolyzed photoresist film (PPF) nonetheless encouraged the search for an alternative starting material.   We found that utilization of the negative photoresist SU 8-2000.5 enabled a higher level reproducibility of film thickness.

In this paper, we use SU 8 C-OTEs to examine the interactions of individual molecules at the electrified carbon/solution interface by drawing on advances of the evanescent wave excitation format in SMS, which allows observation of individual molecules within ~150 nm of a transparent metallic or semi-metallic surface.[20]   Thus, total internal reflection fluorescence microscopy (TIRFM) limits interrogation of the behavior of molecules to within, and only within, this thin interfacial layer.

In addition to reporting on traditional electrochemical and spectroelectrochemical investigations of the newly developed C-OTEs, we also employed what can be called single molecule spectroelectrochemistry (SMSEC) to interrogate the electrosorption behavior of DNA with three different sizes, the largest, being λ-DNA with 48,500 base pairs (48.5 kbp), followed by 7.9 kbp HPV-16, and a 1 kbp fraction of pBR322 DNA being the smallest, we labeled the DNA molecules with POPO fluorescent dye to enable detection with an intensified charge coupled device (ICCD). Choosing different DNA molecules yields insights into size dependent adsorption behavior and how changes in the electrical double layer affect the adsorption.

2. Experimental

The SMSEC experiment combines TIRFM and electrochemistry. The evanescent wave excitation is used to excite the fluorescence of only molecules that are within 130 nm of the electrode surface.

C-OTE Fabrication. The concept of pyrolyzing photoresist to form carbonaceous electrodes stems from the Kinoshita[21] and McCreery[22] laboratories. The basic procedure is detailed in several publications.[21-23] Our fabrication of C-OTEs consists of six steps. First, polished, 500-μm thick quartz substrates (SPI Supplies) are cleaned thoroughly by sonication in acetone, isopropanol, and ethanol, and dried under a stream of high purity nitrogen.

Negative photoresist SU 8 – 2000.5 is then spin coated onto the quartz slides at 6000 rpm for 30 s. Step three soft bakes the coated substrate at 60 °C for two min and then at 90 °C for five min. After cooling, the photoresist is patterned with a broad-band UV light source (31.2 mW/cm^2) for 4 s.

Next, a post exposure bake, step five, occurs for one min at 60 °C, followed by two min at 90 °C to harden the UV-exposed, cross-linked polymer. Using 1-methoxy-2-propanol acetate as the developer and following with isopropanol washes to remove unexposed photoresist, leaves only the desired pattern on the quartz substrate.

Step six pyrolyzes the patterned photoresist film on the substrate in a furnace (Lindberg/Blue M), fitted with a hard-fired alumina tube. A steady stream of forming gas, consisting of 95% high purity nitrogen and 5% hydrogen, is maintained at 1000 sccm throughout pyrolysis and cooling. Temperature ramping occurred at 10 °C/min. The temperature was held constant at three separate times during pyrolysis, first at 80 °C for 40 min to minimize atmospheric oxygen, then at 300 °C for 30 min, and finally at 1000 °C for 1 h. Lastly, the furnace and its contents were allowed to cool to room temperature at a rate no faster than 10 °C/min.

The pyrolyzed electrodes were stored in an ambient laboratory environment for a minimum of three days prior to use. Previous studies showed that the oxygen concentration on the pyrolyzed carbon surface slowly increases over the first three days when exposed to air.[1, 19]

Microchip Preparation. Poly dimethyl siloxane (PDMS), spin-coated at 6000 rpm for 1 min, was cured at 60 °C for 1 h and then mechanically patterned with a razor blade to define the electrode area and a channel for sample introduction. The channel connects to a PDMS reservoir that can accommodate an Ag/AgCl (sat'd KCl) reference electrode and a platinum-wire counter electrode. C-OTE, a No. 1 (170-μm thick) Corning glass cover slip, and PDMS reservoir were assembled with uncured PDMS and two-component epoxy glue and subsequently cured at 60 °C for 1 h. Connection to the working electrode (C-OTE)

employed placement of copper tape onto the edge of the electrode. Minimization of distance above the C-OTE is vital in order to focus the optical microscope onto the surface molecules within the evanescent wave. A schematic of the chip assembly is depicted in Figure 1.

SMSEC Setup. Using index-matching immersion oil (type FF, n = 1.48, Cargill) for airless contact, the assembly was placed on top of the prism. To achieve internal reflectance while optimizing the evanescent wave, the laser beam is directed though the prism at an angle of 66° with respect to the C-OTE. This approach creates a rapidly decaying evanescent wave that penetrates about 120 nm beyond the electrode surface. Light from the laser was removed by an equilateral prism and a pinhole placed prior to the entrance to the observation region. The total laser power, prior to the prism, is ~10 mW. A Zeiss 40x Plan-Neofluar objective was coupled to the assembly with index-matching immersion oil.

An intensified CCD camera (Cascade, Roper Scientific), cooled at -35 °C, was used to record images. The digitization rate of the CCD camera was 1 MHz (16 bits). The frame-transfer function of the CCD camera was operated in the external synchronization mode via a shutter driver/timer (Uniblitz ST 132, Vincent Associates). The CCD exposure frequency was 2 Hz. The exposure time for each frame was 10 ms. The frame sequence was acquired with WinView 32 software (Princeton Scientific).

Electric Double Layer and the Evanescent Wave. The evanescent wave decays exponentially as it protrudes past the electrode surface into the solution,[24, 25] which generally argues that the strongest fluorescence is observed for molecules closest to the surface. Molecules beyond the double layer can also be excited because the evanescent wave actually extends well past the electric double layer. However, the decay of the electrified field

indicates that the contribution of fluorophores beyond the double layer will be relatively small.

Analytes. Three different analytes were used, each suspended in a 10 mM Gly-Gly buffer at pH 8.2. One analyte is 20 pM λ-DNA (Life Technologies), which has 48,502 base pairs (48.5 kbp) and can reach a fully extended length of ~16 μm. Two smaller analytes were also used to investigate the effect of size on molecule interactions at electrified interfaces. The medium sized HPV-16 contains 7.9 kbp is used in a 50 pM concentration, and the third analyte is a 1-kbp fraction of pBR322 DNA at 250 pM.

The DNA samples were labeled with POPO-3 fluorescent dye molecules (Molecular Probes) using a ratio of approximately one dye per five base pairs. The excitation wavelength is 532 nm using a NdYAG laser. The POPO fluorescent label has a maximum absorption at 534 nm and a maximum emission at 570 nm.

3. Results and Discussion

In general, applying a positive potential (e.g., +1.5 V) should electrostatically attract DNA. Because the potential of zero charge (PZC) for many carbon electrodes is near -100 mV,[4] it is expected that negatively charged molecules like DNA will be attracted to the electrode when the applied potential, E_{app}, is positive relative to the PZC. Each of the three sizes tested, ranging from 1 kbp to 48.5 kbp, can be observed as they approach and appear to adsorb to the C-OTE surface.

While switching to a negative applied potential decreases the number of DNA adsorbed within the observation area, the loss is relatively small. Comparing the level of adsorption upon return to the open circuit potential (OCP, -110 mV vs. Ag/AgCl) after

application of a positive potential, more DNA remains adsorbed to the C-OTE than found at the onset of the experiment. This finding, while not fully expected, indicated that other interactions (e.g., hydrophobic) are also of importance.[20, 26] "Sticky ends" on λ-DNA, for example, have been shown to preferentially bind to hydrophobic sites present on the surface.[26]

Data Analysis. Figure 2 presents a portion of the results obtained by switching the applied potential from -1.0 V (2a) to +1.0 V (2b) and then to -1.5 V (2c). The average fluorescence intensity of the observed λ-DNA is graphed in figure 2d. The data show an initial increase in DNA attraction at -1.0 V. Interestingly, application of a positive potential first creates an apparent loss of DNA that is soon overcome by adsorption of single molecules to the electrode surface. We suspect the supporting electrolyte contributes to this behavior. Compared to the large, slower moving DNA, the electrolyte can respond more quickly to changes in surface charge density, and may displace some of the DNA weakly held in the electric double layer. We plan to carry out an electrolyte concentration dependence study to examine this probability more closely.

Only when testing an unused C-OTE, i.e., one that has not yet been subjected to a positive valued E_{app}, is it possible to observe the repulsion of molecules at a negative value of E_{app}. Figure 3 shows the behavior of HPV molecules at OCP (3a) and while applying -2.0 V (3b), with the average fluorescence intensity in the observation region given in figure 3c. As demonstrated in figure 2, once a positive potential has been applied to the electrode, the expected desorption and repulsion of molecules at negative potentials is not significant. This result indicates the specific adsorption sites activated by a positive applied potential remain in force at negative applied potentials.

Surface Oxidation. Various adsorption sites are present on the carbon surface. Some are irreversibly activated by a positive applied potential. Although the oxidation limitation of PPF has been shown to be above +2.0 V by transient techniques like cyclic voltammetry,[27] we also attribute adsorption sites created by the extended application of potentials larger than +0.9 V to surface oxidation. Moreover, the lack of significant response upon discontinuation of a positive applied potential indicates that the adsorption likely occurs at surface oxides and related structural defects.

The permanency of adsorption sites after application of a positive potential is demonstrated in Figure 4, which presents observations for 1 kbp DNA molecules over time and changes in potential. Adsorption behavior remains the same when repeatedly switching the potential between +0.8 V, OCP and –0.8 V. However, once the potential is increased to +1.5 V, the number of adsorption sites appears to increase with time. We attribute the further increase in signal when E_{app} is stepped to +1.5 V to the gradual oxidation of the carbon surface, which creates sites that more strongly interact with DNA. Upon switching back to a negative applied potential (4f), the response does not return to the same level found before the application of +1.5 V. Again, it appears that once these adsorption sites are generated, they continue to play an important role even at applied potentials less than +1.5 V.

Carbon Structure. A closer look at individual adsorption events enables speculation about the heterogeneous structure of carbon by drawing on widely accepted descriptive models.[3, 4] Glassy carbon, for example, is thought of having randomly oriented bands of graphitic carbon throughout, having a surface of both edge and basal planes.[3] Highly oriented pyrolytic graphite (HOPG) on the other hand, consists of well organized, evenly

spaced layers of graphitic sheets, with a small number of surface defects in the surface basal plane. [3]

Electrodes fabricated by pyrolyzing photoresist are described as amorphous carbon with embedded microcrystalline graphitic carbon.[28] The electrochemical characteristics and performance are influenced by the actual structure of the electrode material, and is therefore different for various types of carbon electrodes. Surface defects and edge plane sites are much more likely to serve as electrochemically active sites. Basal planes without defects, as found for HOPG, are highly unreactive. Paying close attention to the location of adsorption events at the C-OTE surface reveals that reversible adsorption occurs repeatedly at the same locations. These locations are assumed to be electrochemically active surface sites, some of which are likely activated through oxidation at defects and edge plane sites.

Defects and surface functional groups may not be the only adsorption sites. Upon application of increasingly positive potential, molecules adsorb in close proximity of previously adsorbed DNA. These adsorption events are attributed in part to the electronic disturbance around defect sites as described by McDermott and McCreery.[8, 9] In STM studies using GC and HOPG, they demonstrated that adsorption is also prevalent in locations in close proximity to a defect. Adsorption at these secondary sites is attributed to electrostatic interactions.[29]

The phenomenon of adsorption in close proximity to defects is nonetheless difficult to track in individual images. This observation is much more apparent when viewing a continuous data stream (see the movie available at www.acs.org). As becomes evident when using λ-DNA with a applied potential above +1.5 V, the initially occupied adsorption sites

appear as nuclei for island formation. Additional molecules adsorb in close proximity of previously adsorbed DNA.

Molecular Size Contribution. Comparisons between the three different sizes of DNA indicate that molecular size influences adsorption. Larger molecules like λ-DNA were found to be attracted to the surface at a lower applied potential when compared to smaller molecules. These observations (see below) were carried out using potential step experiments.

While exact cutoffs in the applied potential at which the three differently sized DNA molecules adsorb could not be determined, the order of adsorption can be detailed. That is, λ -DNA with 48,500 base pairs adsorbs first, followed by HPV-19 DNA with its 7.9 kbps, and the 1 kbp fraction of the pBR322 DNA when systematically increasing the applied potential from 0 to +2.5 V.

These observations are attributed in part to the molecular size and its effect on mass transfer. Diffusion, Brownian motion, and any lateral liquid flow affect the movement of DNA molecules. Because of their size, larger DNA molecules respond more slowly to changes in attractive/repulsive forces. Figure 5 demonstrates that once a section of the λ-DNA is adsorbed, it can partially uncoil. Smaller molecules, on the other hand, respond more quickly and to a larger relative extent to changes in the system.

Our data show that immediately after changing the applied potential from OCP or negative to a positive potential, the background fluorescence in the images decreases. Considering that the DNA molecules have an overall negative charge, this dimming in signal is likely not caused by a direct response of DNA molecules to the positive applied potential,

but rather by the faster moving electrolyte species, which may competitively displace DNA at short times.

The observations for λ-DNA indicate that overall negatively charged molecules are attracted to the electrode surface to a small degree at a negative applied potential. The increase in intensity is caused either by molecules within the electrical double layer, or by λ-DNA outside the diffusion layer but still within reach of the evanescent wave. To improve viewing this possibility, the images in figure 6 are inversed in tint so the black spots denote molecules. Using the large λ-DNA as an example of slower dynamic behavior, we can observe four distinct occurrences upon changes in the surface charge density via applied potential. Figure 6a depicts the surface concentration at OCP. A relatively low level of adsorption is observed and remained unchanged for several minutes prior to collection of these images.

When a negative potential of -0.8 V (6b) is applied, the number of molecules within the evanescent wave increases. Switching the applied potential to +0.8 V causes a small, but observable decrease in molecule concentration near the surface (figure 6c) when compared to 6a. While the number of DNA adsorbed to the surface remains relatively unchanged, the decrease of DNA near the surface is attributed to the supporting electrolyte, which dominates correction of the charge imbalance between the surface and the bulk solution, displacing unbound DNA within the evanescent wave.

It is noteworthy that this electrode had been used previously at positive potentials. A decrease in adsorbed molecules when applying a negative potential is therefore not observed. As described previously, observations on unused C-OTEs result in an increase in adsorption of λ-DNA as positive E_{app} is increased.

Observations for the smaller HPV-16 virus and the 1 kbp pBR322 section do not display an increase in fluorescence when a negative potential is applied to a significant extent. To observe an increase in adsorption, the potential must be stepped to higher positive potentials when compared to λ-DNA. An increase in HPV-16 adsorption is achieved when a +1.5 V potential difference is applied. For the even smaller 1 kbp pBR322 fraction, a significant increase in adsorption was not observed until ~+2.0 V. Thus, the smaller molecular size increases the mobility and responsiveness to changes in the electrical double layer.

4. Conclusions

Using negative photoresist SU 8-2000.5 as starting material resulted in a new process for the fabrication of optically transparent carbon electrodes. The dynamic observation of DNA molecules using the combination of TIRFM and electrochemistry by utilizing C-OTEs and their unique characteristics provides interesting details about the adsorption behavior of single molecules. Because the carbon surface contains adsorption sites activated at different applied potentials, the interaction between analyte molecules and the surface is dependent on past conditions. Once activated by a positive applied potential, desorption during subsequent negative applied potentials is limited.

The effectiveness of applied potentials is dependent on the molecular size of the analyte molecule. Larger molecules move slower and take more time to respond to changes in their surroundings, which leads to a more important role for the electrolyte at short times. Examining the behavior of three different sized molecules indicates that the applied potential is not the only significant force that influences adsorption and retention. Smaller molecules

are more susceptible to motion and respond quickly to changes in lateral flow. Electrostatic attraction and subsequent adsorption requires a stronger positive applied potential to overcome other forces present when compared to larger molecules.

5. Acknowledgements

6. References

(1)   Ranganathan, S.; McCreery, R. L. *Analytical Chemistry* **2001**, *73*, 893.

(2)   Harnisch, J. A.; Porter, M. D. *Analyst* **2001**, *126*, 1841-1849.

(3)   McCreery, R. L. In *Electroanalytical Chemistry*; Bard, A. J., Ed.; Marcel Dekker: New York, 1991; Vol. 17, pp 221.

(4)   McCreery, R. L. In *Interfacial Electrochemistry*; Wieckowski, A., Ed.; Marcel Dekker, Inc.: New York, 1999, pp 631-647.

(5)   Kinoshita, K. *Carbon: Electrochemical and Physiochemical Properties*; Wiley: New York, 1988.

(6)   Weisshaar, D., E.; Porter, M., D. *Electrochemistry Communications* **2001**, *3*, 758-761.

(7)   Deinhammer, R. S., The development of novel chromatographic systems utilizing charge-controllable stationary phases for optimization of separations in liquid chromatography Iowa State University, Ames, 1994.

(8)   McDermott, M., T.; Allred McDermott, C.; McCreery, R., L. *Analytical Chemistry* **1993**, *65*, 937-944.

(9)   McDermott, M., T.; McCreery, R., L. *Langmuir* **1994**, *10*, 4307-4314.

(10)   Kuwana, T.; Winograd, N. In *Electroanalytical Chemistry*; Bard, A. J., Ed.; Marcel Dekker, Inc.: New York, 1974; Vol. 7, pp 1-78.

(11)   Heineman, W. R.; Hawkridge, F. M.; Blount, H. N. *Journal of Electroanalytical Chemistry* **1984**, *13*, 1-113.

(12)   Stotter, J.; Haymond, S.; Zak, J. K.; Show, Y.; Cvackova, Z.; Swain, G. M. *Electrochemical Society Interface* **2003**, *12*, 33-38.

(13)   Zudans, I.; Paddock, J. R.; Kuramitz, H.; Maghasi, A. T.; Wansapura, C. M.; Conklin, S. D.; Kaval, N.; Shtoyko, T.; Monk, D. J.; Bryan, S. A.; Hubler, T. L.; Richardson, J. N.; Seliskar, C. J.; Heineman, W. R. *Journal of Electroanalytical Chemistry* **2004**, *565*, 311-320.

(14) Mattson, J. S.; Smith, C. A. *Analytical Chemistry* **1975**, *47*, 1122-1125.

(15) Haacke, G. *Annual Review of Material Science* **1977**, *7*, 73-93.

(16) DeAngelis, T. P.; Hurst, R. W.; Yacynych, A. M.; Mark, H. B.; Heineman, W. R.; Mattson, J. S. *Analytical Chemistry* **1977**, *49*, 1395-1398.

(17) Haymond, S.; Zak, J. K.; Show, Y.; Butler, J. E.; Babcock, G. T.; Swain, G. M. *Analytical Chimica Acta* **2003**, *500*, 137-144.

(18) Petek, M.; Neal, T. E.; Murray, R. W. *Analytical Chemistry* **1971**, *43*, 1069-1074.

(19) Donner, S.; Li, H.-W.; Yeung, E. S.; Porter, M. D. *Analytical Chemistry* **2006**, *78*, 2816-2822.

(20) Li, H. W.; Park, H. Y.; Porter, M. D.; Yeung, E. S. *Analytical Chemistry* **2005**, *77*, 3256-3260.

(21) Kim, J.; Song, X.; Kinoshita, K.; Madou, M.; White, R. *Journal of the Electrochemical Society* **1998**, *145*, 2314-2319.

(22) Ranganathan, S.; McCreery, R. L.; Majji, S. M.; Madou, M. *Journal of the Electrochemical Society* **2000**, *147*, 277-282.

(23) Hebert, N. E.; Snyder, B.; McCreery, R. L.; Kuhr, W. G.; Brazill, S. A. *Analytical Chemistry* **2003**, *75*, 4265-4271.

(24) Moerner, W. E. *The Journal of Physical Chemistry B* **2002**, *106*, 910-927.

(25) Jung, Y. J.; Barkai, E.; Silbey, R. J. *Journal of Chemical Physics* **2002**, *117*, 10980-10995.

(26) Park, H.-Y.; Li, H.-W.; Yeung, E., S.; Porter, M., D. *Langmuir* **2006**, *22*, 4244-4249.

(27) Wang, C.; Jia, G.; Taherabadi, L. H.; Madou, M. *Journal of Microelectromechanical Systems* **2005**, *14*, 348-358.

(28) Kostecki, R.; Schnyder, B.; Alliata, D.; Song, X.; Kinoshita, K.; Koetz, R. *Thin Solid Films* **2001**, *396*, 36-43.

(29) McCreery, R. L.; Ckine, K. K.; McDermott, C. A.; McDermott, M. T. *Colloids and Surfaces* **1994**, *93*, 211.

7. Figures
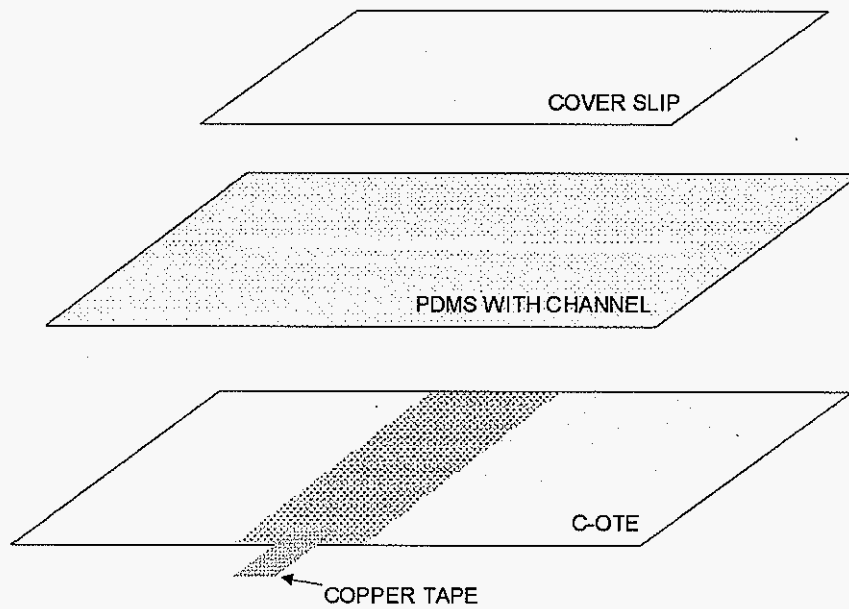
Figure 1. Schematic setup of the C-OTE. PDMS with a mechanically defined channel is sandwiched between a 170 μm thick cover slip and the C-OTE, consisting of a 35 nm thick pyrolyzed photoresist film on a quartz substrate.
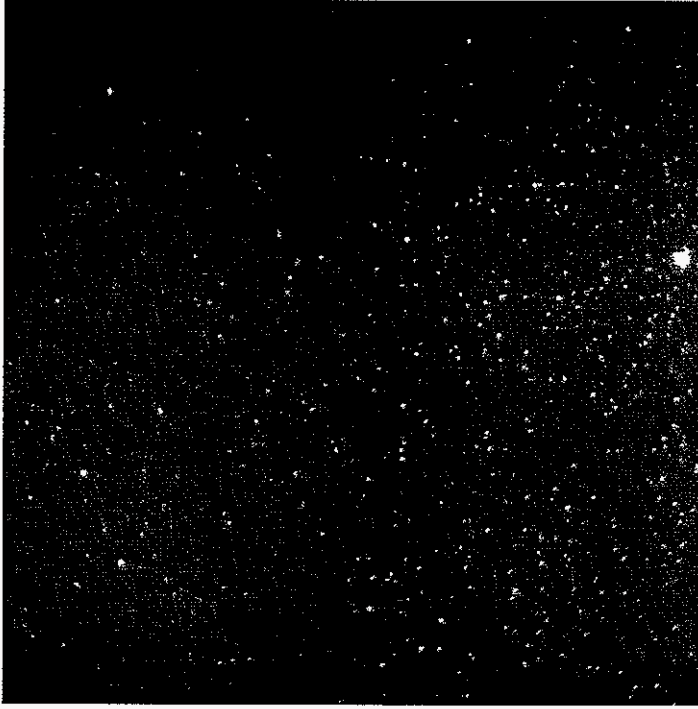
Figure 2a. Electrostatic attraction of 20 pM lambda DNA within 120 nm of 35 nm thick C-OTE, Eapp = -1.0 V.
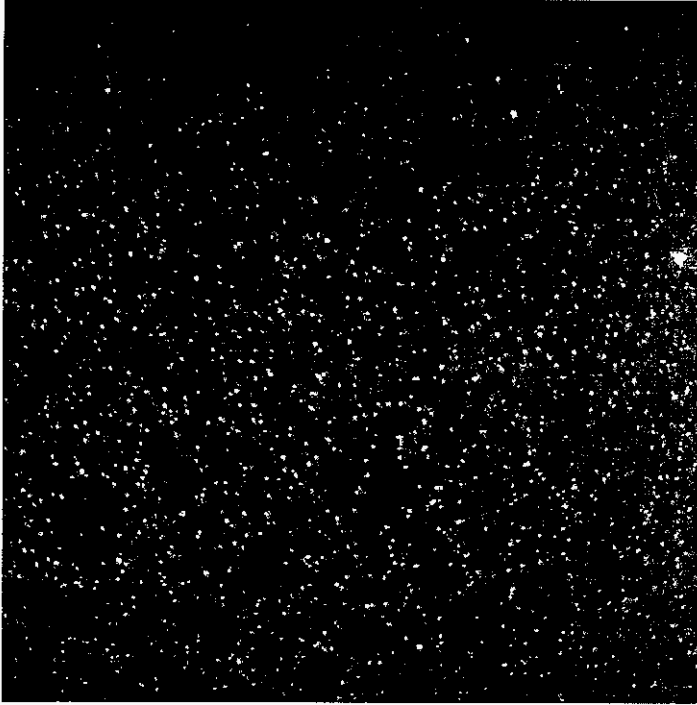
Figure 2 b. Adsorption of 20 pM lambda DNA within 120 nm of 35 nm thick C-OTE, Eapp = +1.0 V.
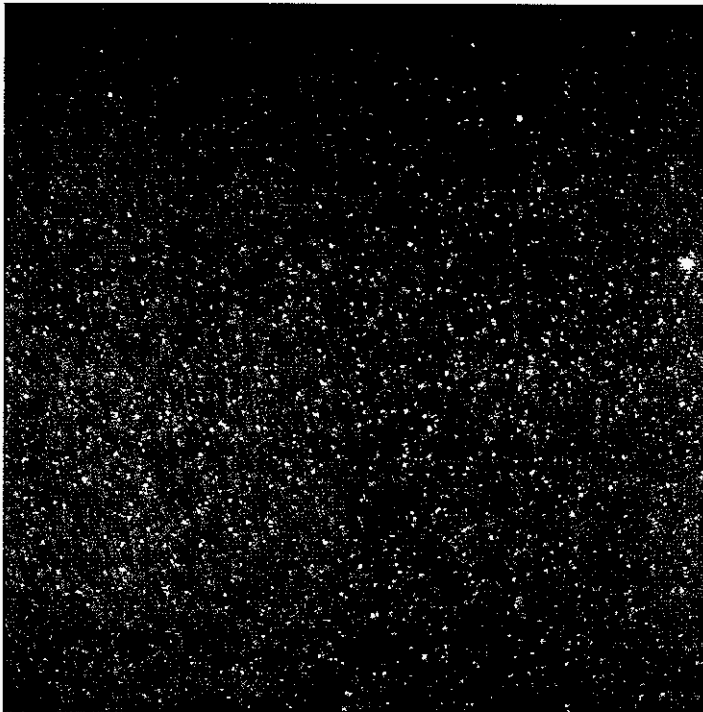
Figure 2 c. Electrostatic attraction of 20 pM lambda DNA within 120 nm of 35 nm thick C-OTE, Eapp = -1.5 V.
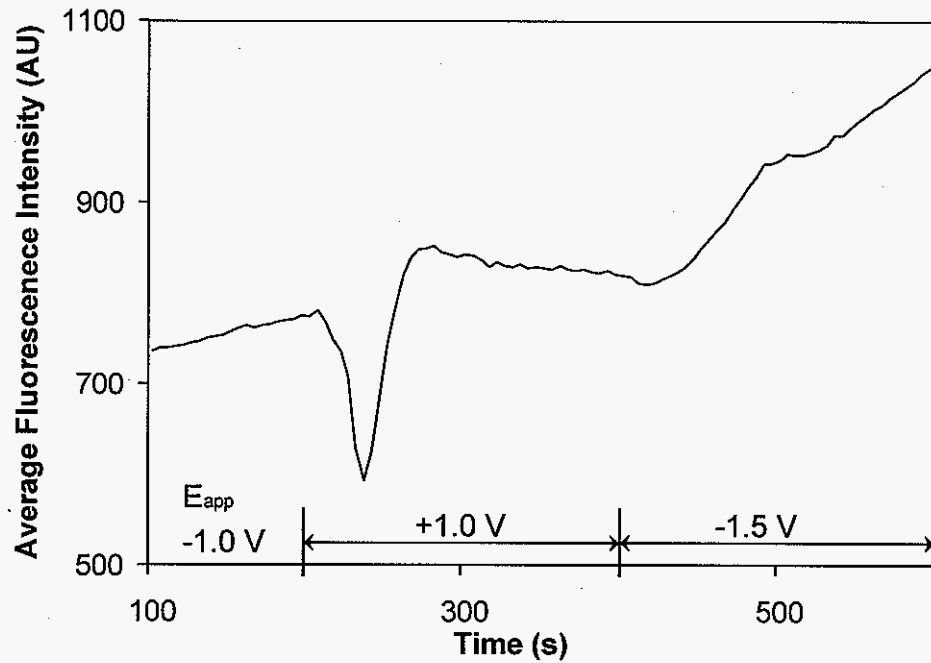
Figure 2d. Average fluorescence intensity of lambda DNA molecules over time while altering the applied potential. Decrease in fluorescence upon switching Eapp from -1.0 V to +1.0 V is caused by restructuring of the electrical double layer.
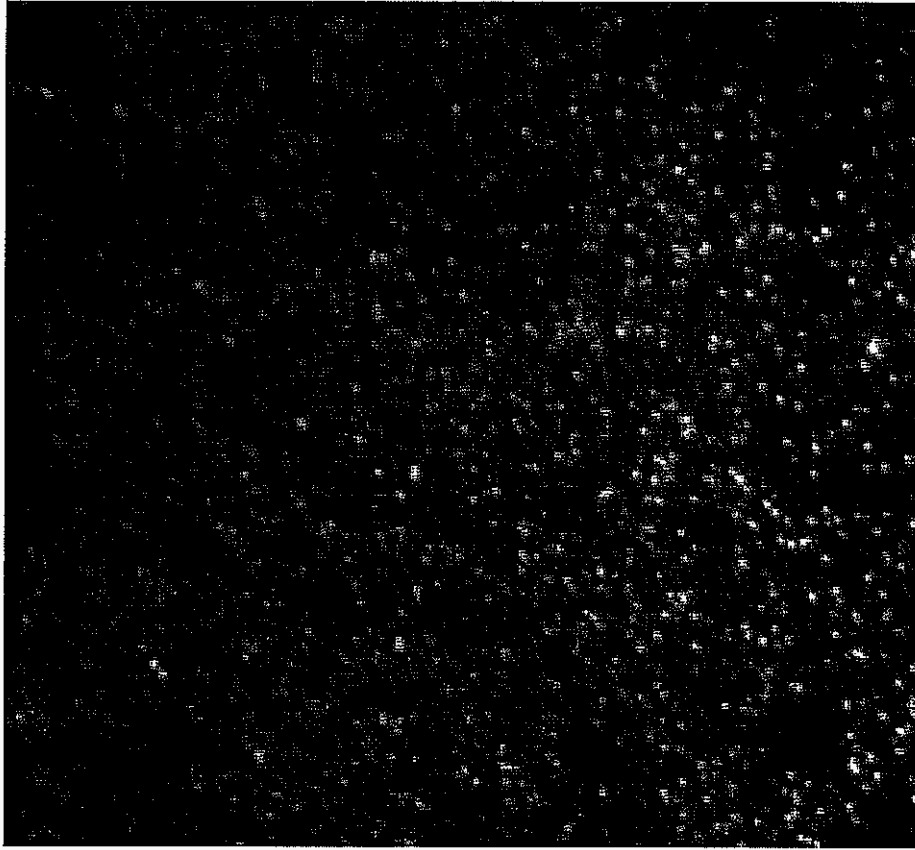
Figure 3a. Adsorption and attraction of HPV-16 molecules to new C-OTE at OCP.
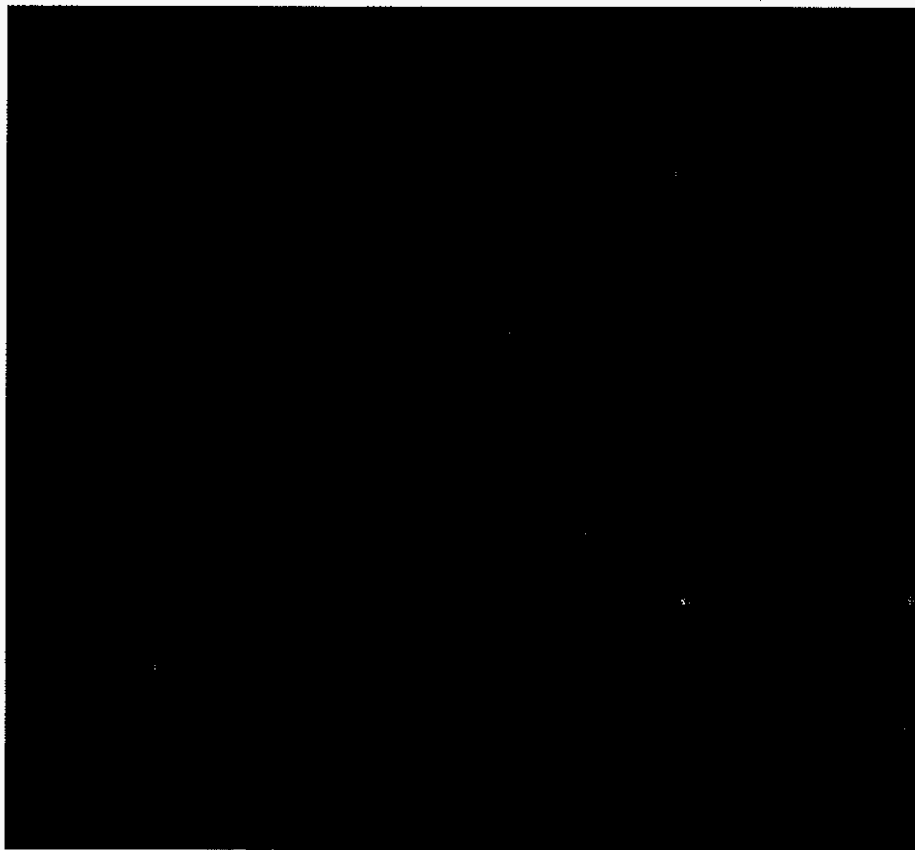
Figure 3b. Desorption and repulsion of HPV-16 molecules from new C-OTE with E_{app} = -2.0 V.
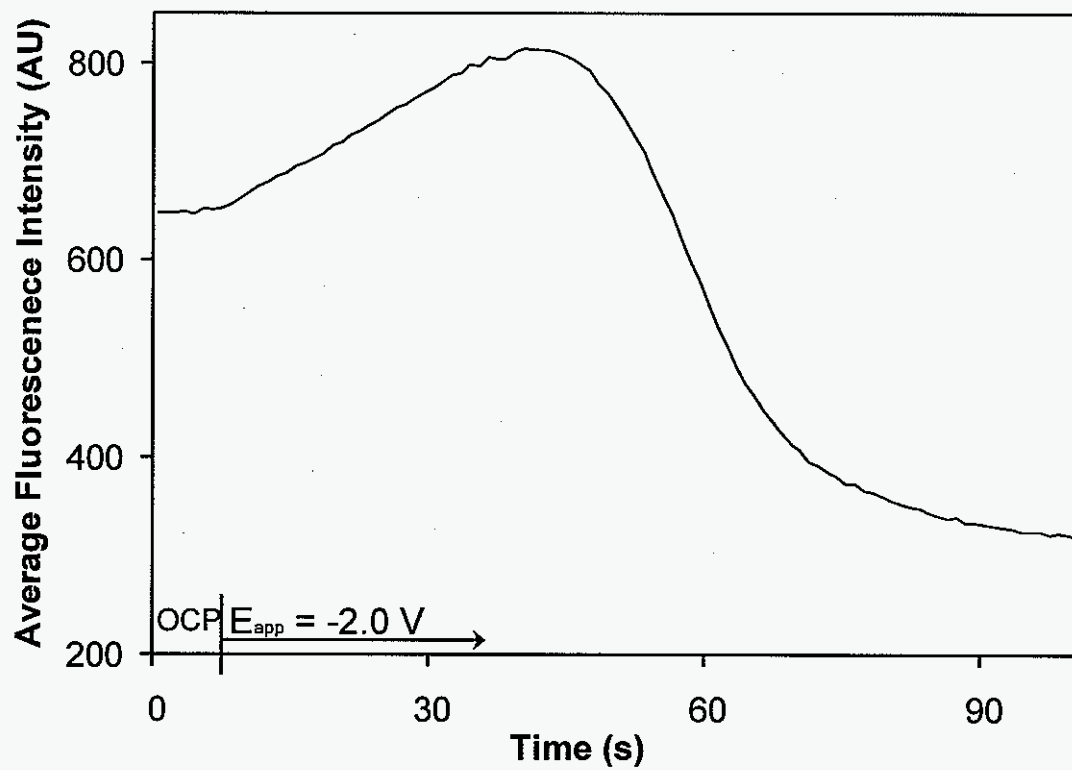
Figure 3c. Fluorescence intensity when the applied potential changes from OCP to -2.0 V. Initial increase in fluorescence is quickly followed by desorption and repulsion of HPV-16 molecules.
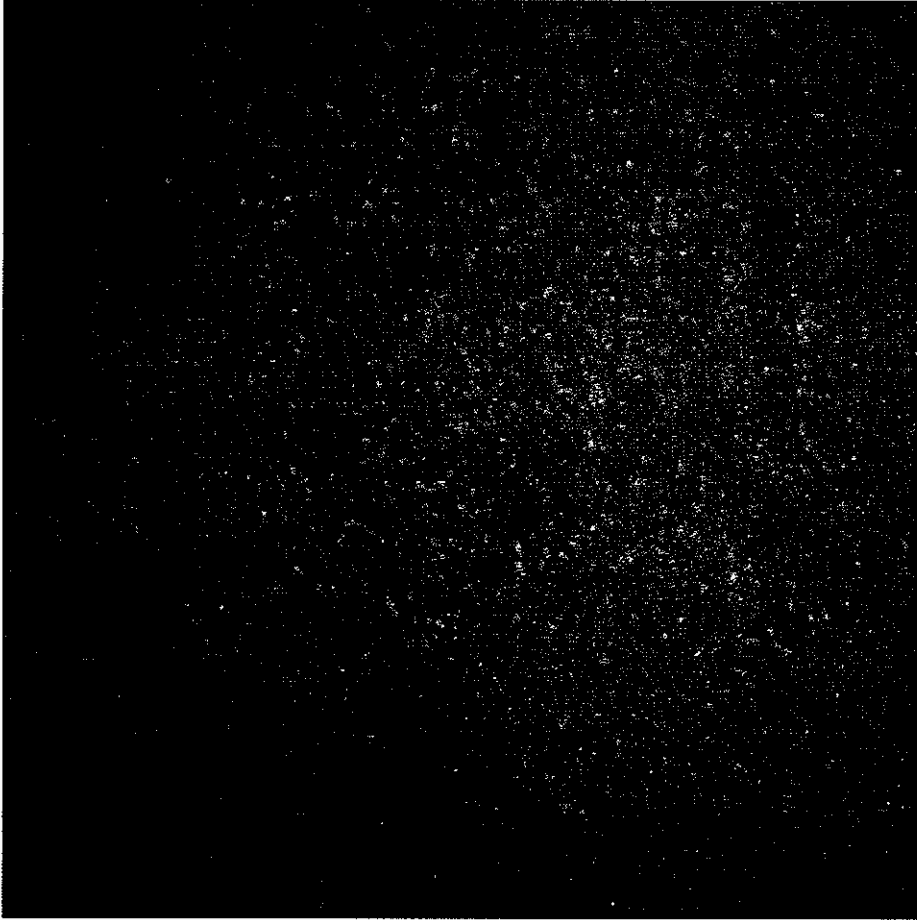
Figure 4a. Fluorescence of 250 pM 1 kbp DNA within 120 nm of C-OTE at E_{app} = OCP.
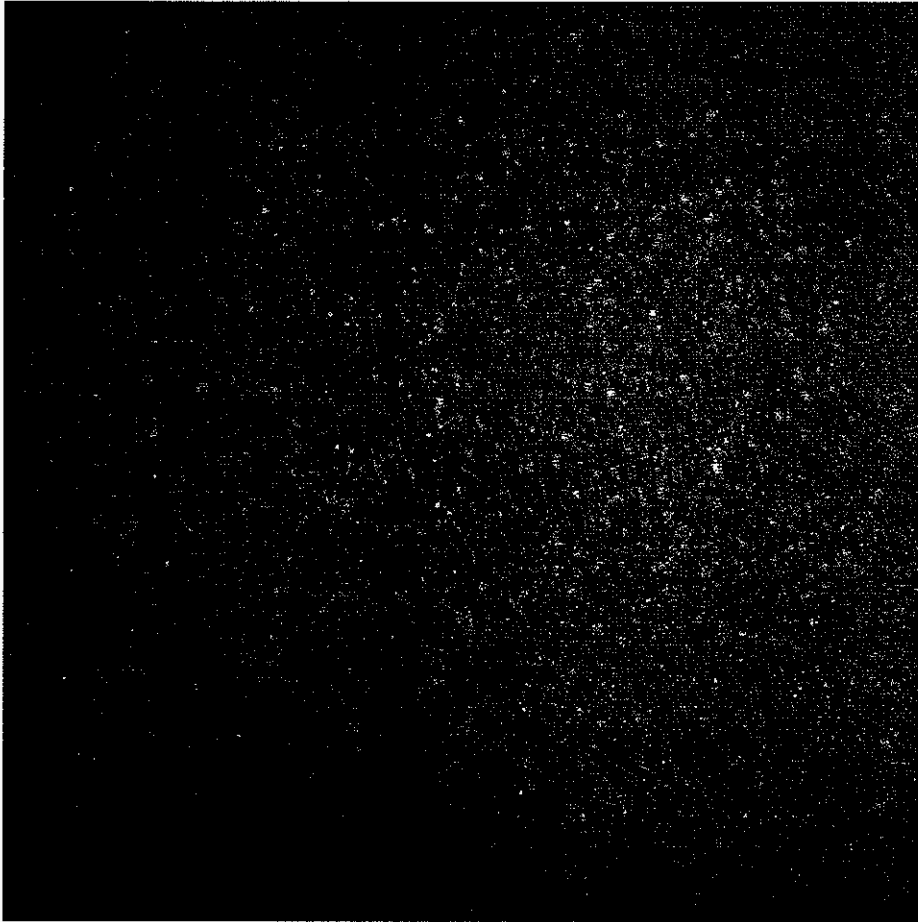
Figure 4b. Fluorescence of 1 kbp DNA within 120 nm of C-OTE at E_{app} = -1.0 V.

**Figure 4c.** Fluorescence of 1 kbp DNA within 120 nm of C-OTE at $E_{app} = +1.0$ V.

Figure 4d. Fluorescence of 1 kbp DNA within 120 nm of C-OTE at E_{app} = -1.5 V.
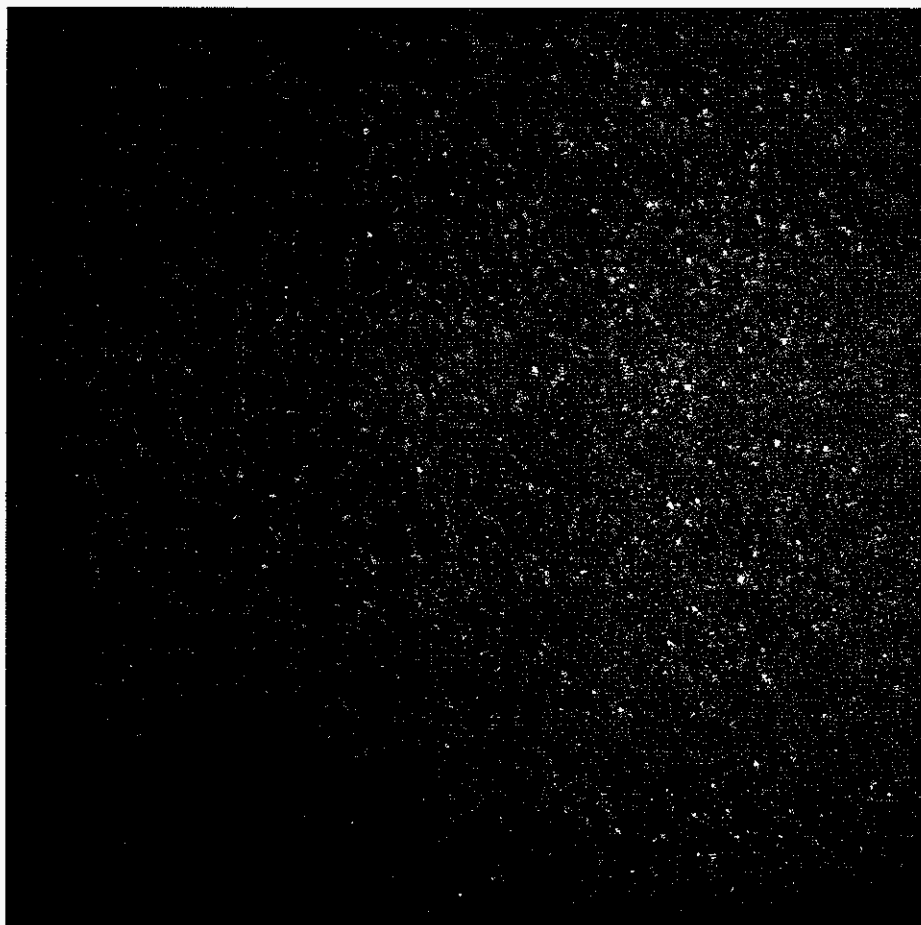
Figure 4e. Fluorescence of 1 kbp DNA within 120 nm of C-OTE at E_{app} = +1.5 V.
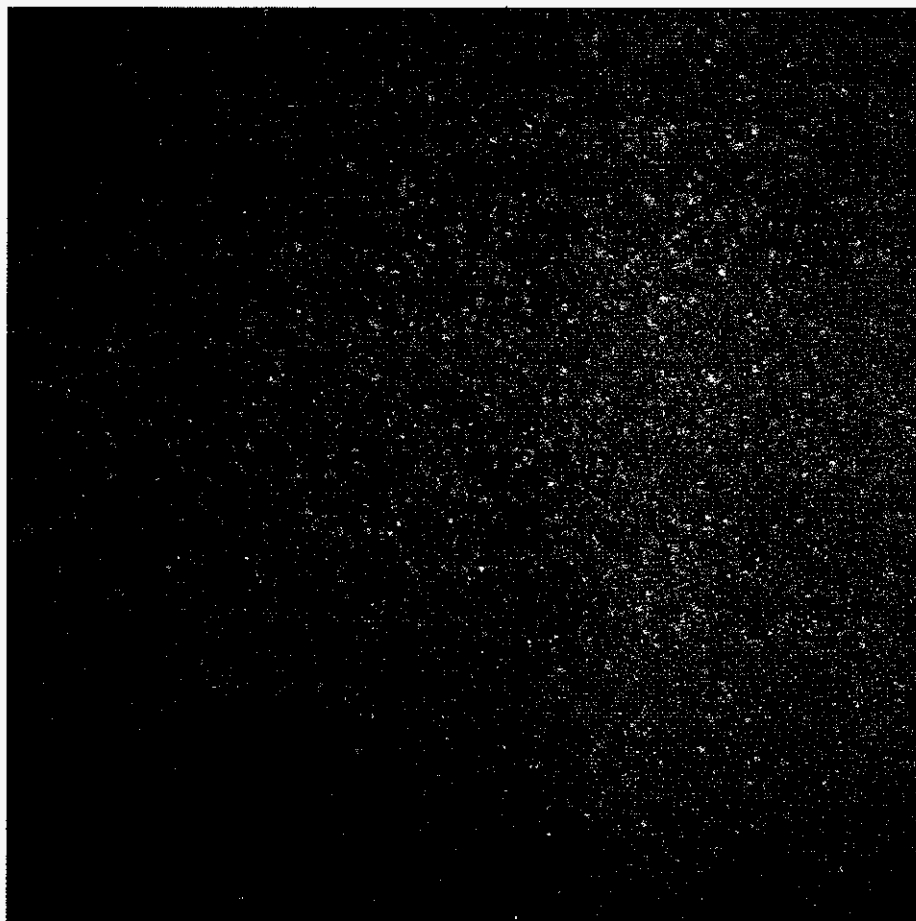
Figure 4f. Fluorescence of 1 kbp DNA within 120 nm of C-OTE at $E_{app} = -2.0$ V
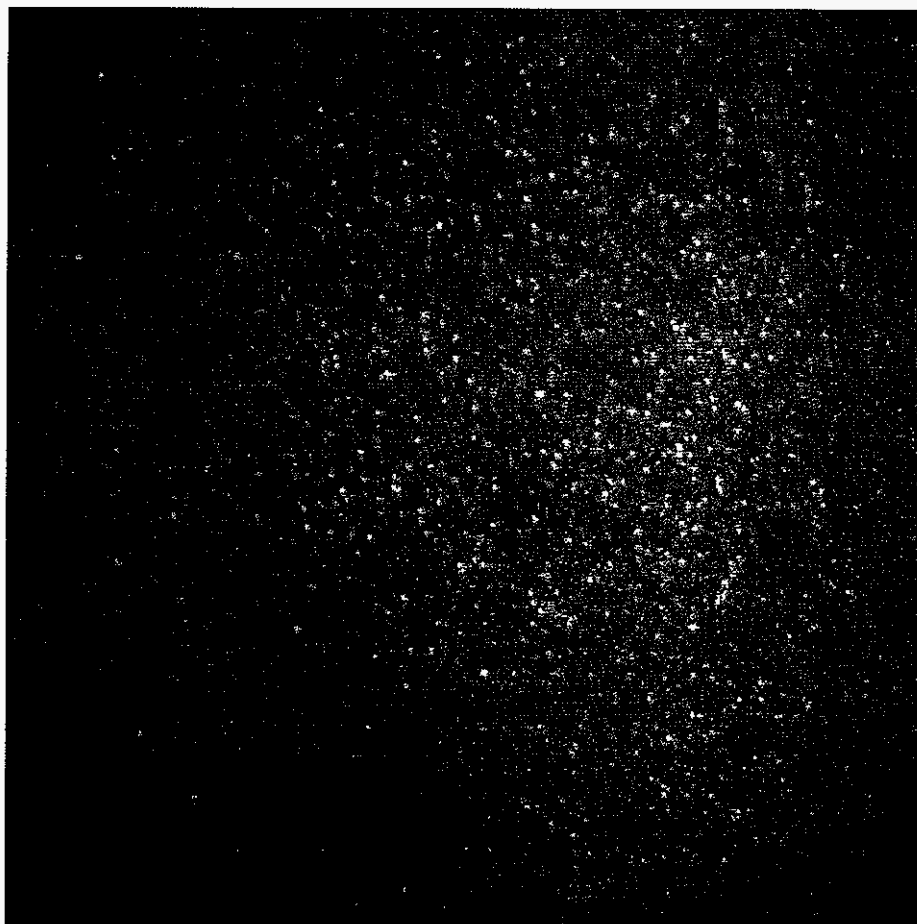
Figure 4g. Fluorescence of 1 kbp DNA within 120 nm of C-OTE at E_{app} = +2.0 V.
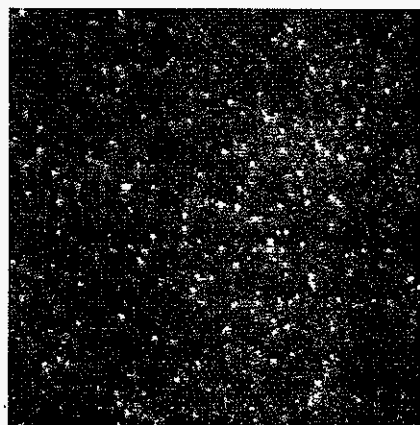
Figure 4h. Close-up of figure 4g. Fluorescence of 1 kbp DNA within 120 nm of C-OTE at E_{app} = +2.0 V.
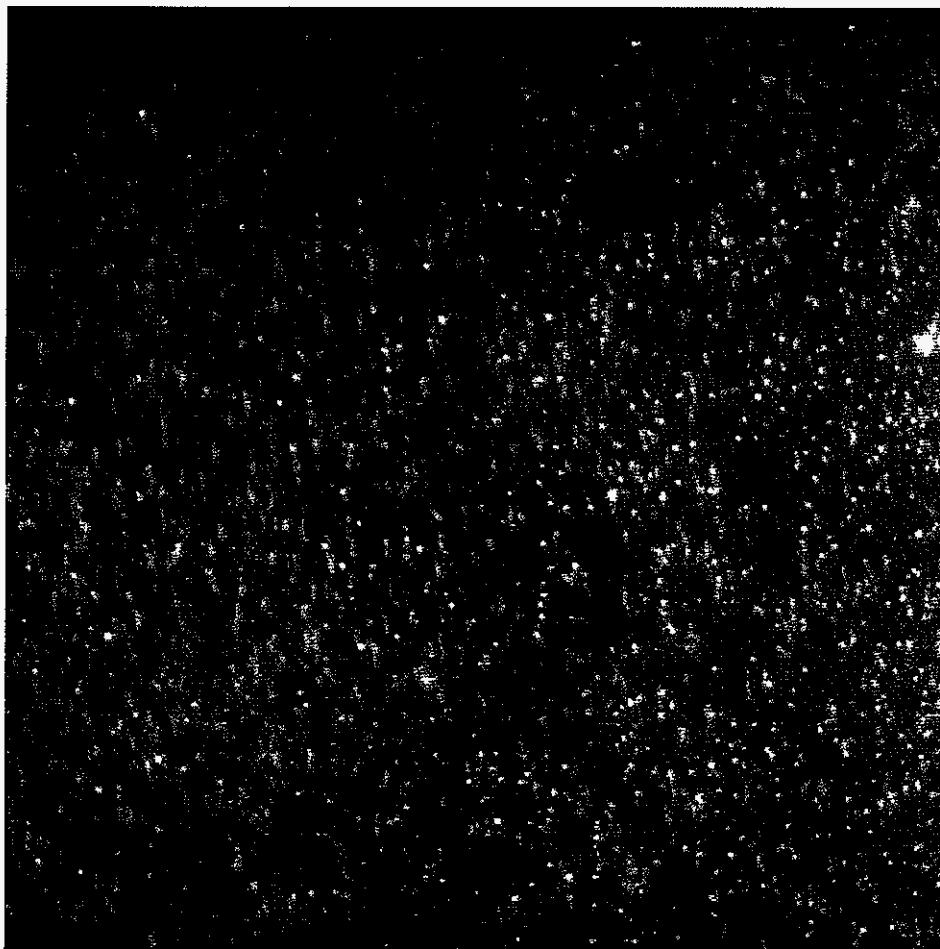
Figure 5. Stretching of λ-DNA when applied potential is switched from -1.0 V to + 1.0 V. λ-DNA adsorbs first with "sticky end".
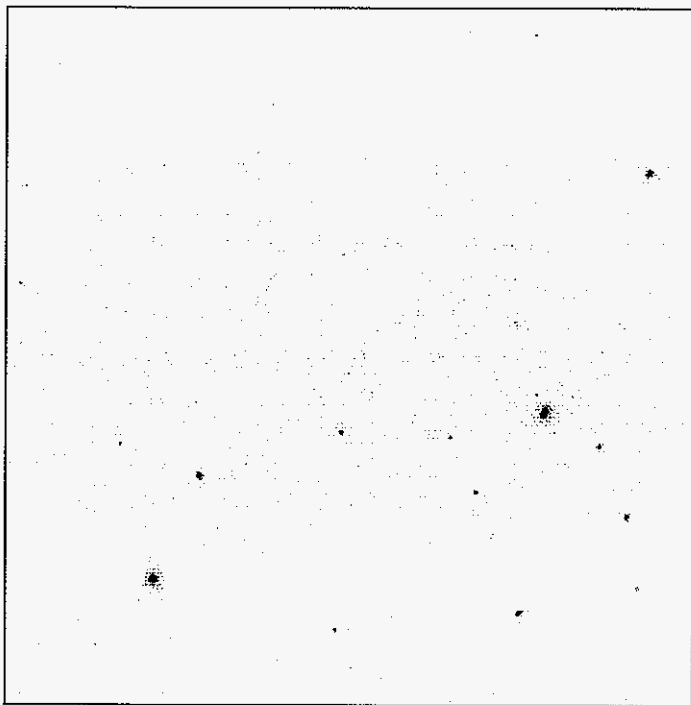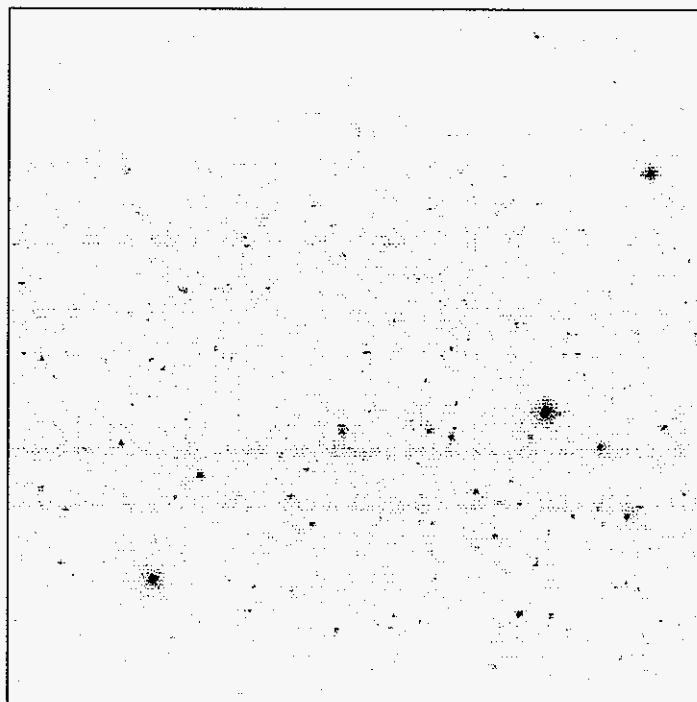
Figure 6a. Adsorption of 50 pM λ-DNA to used C-OTE at E_{app} = OCP.

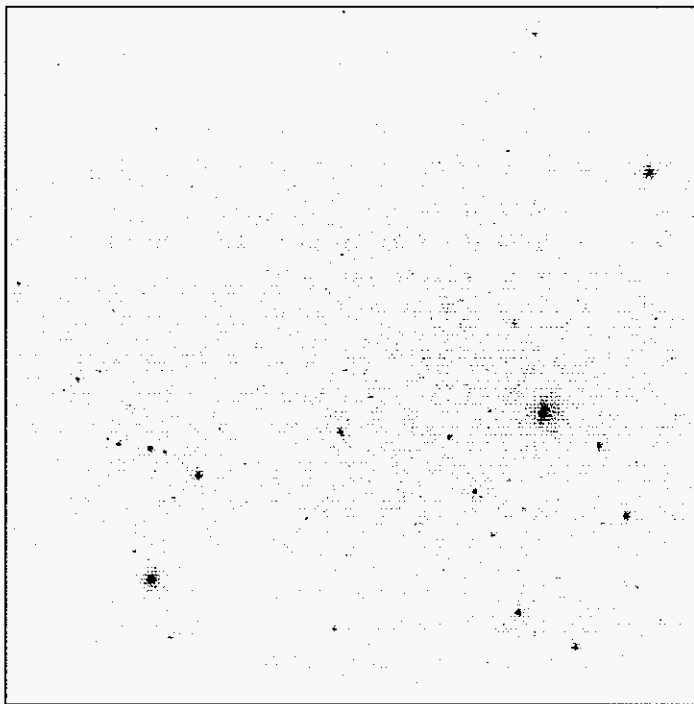**Figure 6b.** Electrostatic attraction of 50 pM λ-DNA to used C-OTE at E_{app} = -0.8 V.

Figure 6c. Repulsion of unbound 50 pM λ-DNA from used C-OTE at E_{app} = +0.8 V.

CHAPTER 4. FABRICATION OF CARBON-BASED OPTICALLY TRANSPARENT MINIGRID ELECTRODES

Sebastian Donner[a] and Marc D. Porter[a,b,]*

[a]Ames Laboratory – U.S.D.O.E., Department of Chemistry, and the Institute for

Combinatorial Discovery, Iowa State University, Ames IA 50011

[b]Department of Chemistry and Chemical Engineering, University of Utah, Salt Lake City,

UT 84112

*Corresponding Author Marc D. Porter, Phone: (801) 587-8325, marc.porter@utah.edu

Abstract

This paper details the fabrication, characterization, and testing of minigrid-type optically transparent electrodes based on the pyrolysis of photopatterned photoresist. More specifically, conductive and electrochemically active minigrids, referred to as carbon-grid optically transparent electrodes (CG-OTEs), are created when positive photoresist AZ P4330RS is spin coated onto a quartz substrate, photolithographically patterned, and subsequently pyrolyzed at 1000 °C in a reducing atmosphere. The resulting voids in the carbonized grid-like material function in a manner similar to that of a neutral density filter, and transparencies of 80% have been achieved. The design, material characterization, and results from the spectroelectrochemical performance of this system using hydroxymethyl ferrocene and ferro/ferricyanide are discussed.

1. Introduction

Optically transparent electrodes (OTEs) have aided the investigation of electrochemical processes for more than 40 years [1-3]. As first conceived and reported by Kuwana, Darlington, and Leedy in 1964 [4], many of the early formats for OTEs entailed the deposition of a thin layer of conductor on an optically transparent substrate. The design of an OTE therefore relies on an inverse correlation between optical transparency and conductivity [1, 2, 5-10], which generally limits film widths to the ~100 nm.

Metallic microscreens, also known as minigrid electrodes, represent another widely used construct in spectroelectrochemical investigations [3]. The optical transparency of minigrid electrodes derives from the voids in the microscreen. Like a neutral density filter, the grid density can be varied to adjust the transparency of the electrode by changing the distance between the wires of the screen and/or the width of the wires.

There are two other important aspects of minigrid OTEs. First, minigrid electrodes have a low internal ohmic resistance. Low resistances minimize, if not eliminate, the onset of a potential distribution across the electrode surface, [8] which may complicate experiments with thin-film type OTEs. Second, the delivery of reactant to the mesh-like electrode has a uniquely different temporal evolution with respect to the semi-infinite linear diffusion process at a planar electrode [3]. At short times, linear diffusion conditions dominate. However, as electrolysis proceeds, the diffusion profile becomes nonlinear as the diffusion layers between the grids begin to intersect, and the reactant in the voids becomes fully

depleted at a time dependent on the distance between gridlines. Eventually, the diffusion layer thickness grows larger than the void and grid dimensions, and the merging concentration profiles from the grids again resemble linear diffusion.

The present paper builds on advances detailed by various laboratories on the preparation of carbon electrodes by the pyrolysis of photoresist films (PPF) [11-14]. Along these lines, we recently described an approach that used the pyrolysis of thin (10-80 nm) films of the photoresist AZ 4330, supported on quartz substrates, for the fabrication of optically transparent carbon electrodes [15]. We showed that the pyrolysis process yielded mechanically robust, amorphous carbon coatings, which could be readily incorporated into conventional and single molecule spectroelectrochemical studies.

The work herein takes a different tactic towards the integration of carbon in spectroelectrochemistry by first photopatterning the spin-coated photoresist into a quartz-supported minigrid layout that is then pyrolyzed in a reducing atmosphere at 1000 °C to form a carbon-grid optically transparent electrode (CG-OTE). The following details the preparation, characterization, and spectroelectrochemical application of these CG-OTEs.

2. Experimental

2.1. CG-OTE Fabrication

The preparation of CG-OTEs consists of six steps, which, with the exception of photopatterning, follow those described by the Kinoshita [12] and McCreery [11] laboratories. Our procedure begins by cleaning a quartz substrate (2.54 x 2.54 cm) with acetone, isopropanol, and ethanol. The substrate is then dried under a stream of high-purity nitrogen.

Next, as-received positive photoresist AZ P4330-RS (AZ Materials, Somerville, NJ, USA) is spin coated onto the quartz substrate at 6000 rpm for 30 s. Step three "soft bakes" the coated substrate for three min at 90 °C to drive solvent from the photoresist film, improve adhesion of the coating to the substrate, and anneal shear stresses due to spin coating. In step four, the coated substrate is brought into light contact with a photomask and then patterned with a 31.2 mW/cm^2 broadband, UV light source (ABM Inc., San Jose, CA, USA) for 6 s. The chromium masks were designed with AutoCAD$^®$ and fabricated by Microtronics Inc. (Newtown, PA, USA).

Step five dissolves the irradiated photoresist by immersing the samples with gentle agitation in a 1:4 dilution (v/v) of AZ 400 K developer (AZ Materials, Somerville, NJ, USA). Care must be taken, however, to avoid vigorous agitation, which can distort the pattern, fracture the grids, and induce delamination.

The final step pyrolyzes the patterned photoresist. The samples are placed in a furnace (Lindberg Blue M, New Columbia, PA, USA), fitted with a hard-fired alumina tube. The tube is flushed with forming gas (95% high-purity nitrogen:5% hydrogen (v/v)) while ramping the temperature to 100 °C at 10 °C/min. The temperature is then held at 100 °C for 40 min to minimize the presence of gas-phase oxygen and to eliminate solvent and water. Subsequently, the temperature is ramped by 10 °C/min to 1000 °C and held there for 1 h. Thereafter, the furnace is cooled to room temperature at a controlled rate that is not greater than 10 °C/min in order to avoid cracking the pyrolyzed photoresist which can be caused by abrupt temperature changes. The flow of the forming gas is maintained at 1000 sccm throughout the entire pyrolysis process.

2.2. Instrumentation

Electrochemical experiments employed an Electrochemical Analyzer model CHI 600A (CH Instruments, Austin, TX, USA). A platinum wire acted as the counter electrode, and a silver/silver chloride (Ag/AgCl, saturated KCl) electrode served as the reference electrode. Ferrocyanide and hydroxymethylferrocene (HMF), both obtained from Aldrich (St. Louis, MO, USA), were used to assess the performance of the CG-OTEs. This couple has a formal reduction potential at +0.26 V (vs. Ag/AgCl, saturated KCl) in 1.0 M potassium chloride (KCl). The electrochemical experiments were performed without *iR* compensation.

Absorbance measurements utilized a HP 8453 UV-visible spectrometer (Agilent, Santa Clara, CA, USA) and were corrected for contributions from the underlying quartz substrate. Spectroelectrochemical studies were performed using the classic cell design of Kuwana and Winograd [1]. An O-ring (6.0 mm) sealed the CG-OTE to the cell and defined the geometric area of the substrate exposed to solution (0.28 cm^2). Conductive copper tape, positioned around the outside of the O-ring, served as the electrical contact to the potentiostat. The probe beam was oriented normal to the electrode surface.

The thickness of the coatings was determined before and after pyrolysis by using a surface profilometer (Dektak IIA, Sloan, Woodbury, NY, USA).

3. Results and Discussion

3.1. Design

The CG-OTEs were designed to span an area of $\sim 1 \text{ cm}^2$ on the underlying quartz substrate and were surrounded by a 1-cm wide border of unpatterned, pyrolyzed photoresist on all sides. Three different layouts were used. The first is shown in the optical micrograph

in Figure 1a. It consists of a grid that has 5-μm wide lines of pyrolyzed photoresist, which are separated by 100 μm (center-to-center). Electrodes with this pattern are referred to as 5-100G. The second design, denoted 5-100L, consists of 5-μm wide lines that are parallel to each other and have a center-to-center spacing of by 100 μm. This structure is presented in Figure 1b. The third construct, 5-50L, is similar to that of 5-100L, but has a 50-μm offset (center-to-center) between the 5-μm wide lines. An optical micrograph for this design is given in Figure 1c.

As is evident in Figure 1, the sizes and shapes of the CG-OTEs closely follow the lithographic pattern derived from the photomasks. Importantly, the widths of the features in all three layouts prior to pyrolysis remain close to 5 μm after pyrolysis. Maintenance of the pattern dimensions is attributed to both the polymeric nature of the starting material and the pyrolysis process [16, 17]. The polymeric structure of the resist limits spreading as the temperature increases and solvent and unreacted monomers are driven from the coating at low temperature (300 °C), whereas pyrolysis slowly carbonizes (>500 °C) the coating into an amorphous, interwoven network of conductive aromatic rings. The ability to pattern specific features and maintain their size throughout pyrolysis presents a flexible pathway for the fabrication of CG-OTEs with a wide range of architectures.

There is one more important characteristic of these designs. Past experiments established that the resistivity of bulk PPF is ~6 x 10^{-3} Ω-cm [11]. Moreover, a detailed investigation of the conductivity dependence on film thickness carried out in our previous work indicated that the conductivity of PPF stabilizes once the thickness exceeds ~500 nm [15]. Thus, a single spin coating step, which resulted in a post-pyrolyzed line thicknesses of 654±23 nm, proved more than sufficient. A profilometer scan across a line on a 5-50L CG-

OTE is given in Figure 2. The slopes of the side walls reflect the lack of vertical structure preservation caused by the low aspect ratio for positive photoresist [11, 18]. The close-up of the minigrid in Figure 3 visualizes the effect of the polymeric nature of the photoresist in two optical micrographs. During pyrolysis, the photoresist transitions through a softening stage that causes minor smoothening of the shape of photo-patterned features.

3.2 Grid Characteristics

The optical transparency of our CG-OTEs in the UV and visible spectral range, shown in Figure 4, provides a substantial improvement over our earlier C-OTEs [15]. The transparencies are only marginally different since the carbon grids are essentially neutral density filters, these materials are transparent across the UV-VIS-IR range of the electromagnetic spectrum, with the usable window then defined by the optical properties of the substrate, cell, and electrolysis solution. For example, the transparencies for the electrodes at 420 nm are 74%, 80% and 71% for the 5-100G, 5-100L, and 5-50L electrodes, respectively.

The slight increase in transparency at longer wavelengths follows the trend observed with C-OTEs, which have a continuous, transparent carbon film. For the CG-OTEs, this trend is presently attributed to the extremely thin and strongly adhesive layer of carbon that remains affixed to the underlying substrate after pyrolysis.

The cyclic voltammetric response in Figure 5a demonstrates the electrochemical response of a 5-100G CG-OTE when scanning at 1 mV/s in 1.0 mM solution of hydroxymethylferrocene and 1.0 M KCl (aq). The separation in peak-current potentials is 59 mV, which is consistent with the mass transfer (i.e., reversible) response expected for a

kinetically fast redox couple like hydroxymethyl ferrocene/ferrocenium cation. The same peak separations (data not shown) were also consistently observed for the other two types of CG-OTEs. However, the magnitudes of the peak currents differed, with the highest found for 5-50L, the lowest for 5-100L, and an intermediate value for 5-100G CG-OTE. This trend, as detailed in the subsequent discussion of the spectroelectrochemical data, is a direct consequence of how the grid spacing affects the diffusion distances required for transport of the redox reactant. That is, while there are small differences in the actual electrode areas of each CG-OTE, the distance required for a reactant near the substrate (e.g., in a void) to diffuse to the electrode is on average less at 5-50L, followed by 5-100G and 5-100L.

A current-potential curve from a scan in only supporting electrolyte (1.0 M KCl) is shown in Figure 5b. The response points to a usable potential window of ~1.5 V, which may be extended by more fully degassing the solution. The breadth of the working potential window is on par with that of earlier types of carbon electrodes manufactured by the pyrolysis of this photoresist [19, 20].

3.3 Spectroelectrochemical Performance

Chronoabsorptometry experiments using each of the CG-OTE designs were performed to investigate their potential applicability to monitor the change in the optical properties of a redox couple as a function of electrolysis time. These experiments therefore followed the conversion of ferrocyanide (10.0 mM) to ferricyanide in 1.0 M KCl by stepping the applied potential from 0.00 to +0.60 V. These results are exemplified in Figure 6, which shows a portion of the findings using a 5-100G CG-OTE. As expected, the absorbance increases with time because of the conversion of ferrocyanide to ferricyanide (λ_{max} = 420 nm,

$\varepsilon_{max} = 1020$ M^{-1}cm^{-1}) [21]. The results from all three types of CG-OTEs are summarized in Figure 7 as plots of the observed absorbance at 420 nm against the square root of electrolysis time, $t^{1/2}$.

At the onset of the potential step, the response is caused by the ferricyanide generated at the electrode surface as it diffuses into the optical path of the light beam between the grids. At this time, the concentration profile near the surface mimics the perforated character of the electrode design. The oxidation product, ferricyanide, concentration is highest near the electrode surface and decreases quickly as the distance from the surface increases. At locations near the center of the gap between the carbon grids, there is little to no ferricyanide.

Over time, diffusion transports more ferricyanide into the optical path between the lines. Eventually the redox concentration profiles around each grid begin to overlap with the concentration profiles generated at the neighboring grids. This results in a planar concentration profile with respect to the entire CG-OTE, including the voids. The time it takes to obtain a planar concentration profile depends on the dimensions of the grid and its' voids. Using various gold minigrid electrodes, Murray describes the influence of line thickness and width as well as the holes between lines.[3] While we did not investigate all parameters presented for the gold minigrid electrodes, our results demonstrate the same phenomenon described by Murray and his co-workers.

The line width influences the electrode surface area and the transparency of the grid. The former limits the number of redox reactions that can occur at any given time. One way of increasing the electrode surface area is to increase the line thickness while maintaining the line width. Using a photoresist with higher viscosity enables deposition of thicker films which results in thicker lines and increased electrode area while maintaining line width.

Negative photoresist such as SU-8 can be used to manufacture grid electrodes with thicker lines while maintaining transparency. Negative photoresists have a higher aspect ratio which allows the fabrication of tall structures with smaller line width and vertical walls.

The line width can be correlated to the transparency of the grid. In addition to decreasing transparency with increasing line width, the lines block the light path and prevent detection of analyte molecules in the shadows that the lines create. Thus any light absorbing molecules that are generated on top of the electrode in the shadow will not contribute to the absorption response unless they diffuse into the optical path.

Besides the grid electrode area and transparency, the spacing between the lines also influences how quickly a planar concentration profile can be achieved. The closer the lines are placed together, the faster the planar concentration profile is achieved. The observed absorbance changes at the 5-100G grids were slower than for the 5-50L electrodes, but faster than for the 5-100L electrodes. The lower electrochemically active electrode area causes this expected behavior. Comparing transparency and absorbance data makes it evident that closer proximity of lines will decrease the transparency of the grid electrodes while speeding up attainment of a planar concentration profile.

Due to the varying number of lines per area for the different CG-OTE designs, the actual electrode material area is different for each electrode. This results in different temporal profiles for the optical response at the three electrodes. The smaller gap for the 5-50L CG-OTEs results in the most rapid attainment of a planar concentration profile.

The observed absorbance changes at the 5-100G grids were slower than for the 5-50L electrodes, but faster than for the 5-100L electrodes. The lower electrochemically active electrode area causes this expected behavior.

The change in concentration is observed by measuring the absorbance over time. Graphing the absorbance versus the square root of time provides information about the diffusion behavior of the oxidation product, ferricyanide, and how fast a planar concentration profile is achieved. In the time span used for observations presented in this paper, only the 5-50L CG-OTE was able to generate a planar concentration profile. This is reflected by the onset of linearity that can be seen in Figure 7. The linearity of the absorbance response indicates that the semi-infinite linear diffusion model and its formulas can be applied.

The delayed onset of the linear region for the 1-100G and 5-100L CG-OTEs is attributed to the increased distance between the electrode lines when compared to 5-50L electrodes. It is, however, clear that both amount of ferricyanide generated and the onset of a planar concentration profile are directly related to the true geometric surface area of the electrode material. Optimization of CG-OTEs will involve the fabrication of grids with thicker lines that are placed closer together and have a smaller line width.

4. Conclusions

The fabrication of CG-OTEs provides a suitable alternative to C-OTEs. Improved transparency and adequate conductivity of these electrodes are two advantages. The ability to pattern the photoresist lithographically enables facile adjustments in the size and shape of the electrode structure. For CG-OTEs, the separation distance between lines as well as the line width can be altered to influence the transparency of electrodes. Emergent technology now allows the preparation of photoresist features at nanometer length scales, and experiments along these lines are planned.

92

Using photoresists with different viscosities or alterations of the deposition scheme can also influence the thickness of minigrids. Features with a high aspect ratio for thicker patterns can be achieved by using a negative photoresist like SU 8. This enables fabrication of well-defined features with walls more perpendicular to the substrate [18], thus increasing electrode area without decreasing transparency. Maintaining the shape and dimensions of the photopatterned features throughout fabrication and pyrolysis enables accuracy and reproducibility.

Instead of tedious preparation of different grids for metallic minigrid electrodes, fabrication of CG-OTEs can be easily adjusted by changing the mask used in the exposure process. Different grids can be developed and pyrolyzed simultaneously. Multiple grid patterns can even be applied to the same substrate. Expansion of the CG-OTE functionality to the infrared spectral region by moving to a suitably transparent substrate is underway.

5. Acknowledgements

7. References

[1] T. Kuwana and N. Winograd, in A.J. Bard (Editor), Electroanalytical Chemistry, Vol. 7, Marcel Dekker, Inc., New York, 1974, p. 1.

[2] W.R. Heineman, F.M. Hawkridge and H.N. Blount, Electroanalytical Chemistry, 13 (1984) 1.

[3] M. Petek, T.E. Neal and R.W. Murray, Anal. Chem., 43 (1971) 1069.

[4] T. Kuwana, R.K. Darlington and D.W. Leedy, Anal. Chem., 36 (1964) 2023.

[5] J. Stotter, S. Haymond, J.K. Zak, Y. Show, Z. Cvackova and G.M. Swain, Electrochem. Soc. Interface, 12 (2003) 33.

[6] I. Zudans, J.R. Paddock, H. Kuramitz, A.T. Maghasi, C.M. Wansapura, S.D. Conklin, N. Kaval, T. Shtoyko, D.J. Monk, S.A. Bryan, T.L. Hubler, J.N. Richardson, C.J. Seliskar and W.R. Heineman, J. Electroanal. Chem., 565 (2004) 311.

[7] J.S. Mattson and C.A. Smith, Anal. Chem., 47 (1975) 1122.

[8] G. Haacke, Ann. Rev. Mater. Sci., 7 (1977) 73.

[9] T.P. DeAngelis, R.W. Hurst, A.M. Yacynych, H.B. Mark, W.R. Heineman and J.S. Mattson, Anal. Chem., 49 (1977) 1395.

[10] S. Haymond, J.K. Zak, Y. Show, J.E. Butler, G.T. Babcock and G.M. Swain, Anal. Chim. Acta, 500 (2003) 137.

[11] S. Ranganathan, R.L. McCreery, S.M. Majji and M. Madou, J. Electrochem. Soc., 147 (2000) 277.

[12] J. Kim, X. Song, K. Kinoshita, M. Madou and R. White, J. Electrochem. Soc., 145 (1998) 2314.

[13] A.M. Lyons, J. Non-Cryst. Solids, 70 (1985) 99.

[14] R. Kostecki, B. Schnyder, D. Alliata, X. Song, K. Kinoshita and R. Koetz, Thin Solid Films, 396 (2001) 36.

[15] S. Donner, H.-W. Li, E.S. Yeung and M.D. Porter, Anal. Chem., 78 (2006) 2816.

[16] O.J.A. Schueller, S.T. Brittain and G.M. Whitesides, Sensors and Actuators A, 72 (1999) 125.

[17] B.Y. Park, L.H. Taherabadi, C. Wang, J. Zoval and M. Madou, J. Electrochem. Soc., 152 (2005) J136.

[18] C. Wang and M. Madou, Biosensors and Bioelectronics, 20 (2005) 2181.

[19] N.E. Hebert, B. Snyder, R.L. McCreery, W.G. Kuhr and S.A. Brazill, Anal. Chem., 75 (2003) 4265.

[20] S. Ranganathan and R.L. McCreery, Anal. Chem., 73 (2001) 893.

[21] J. Skully, P. and R. McCreery, Anal. Chem., 52 (1980) 1885.

8. Figures

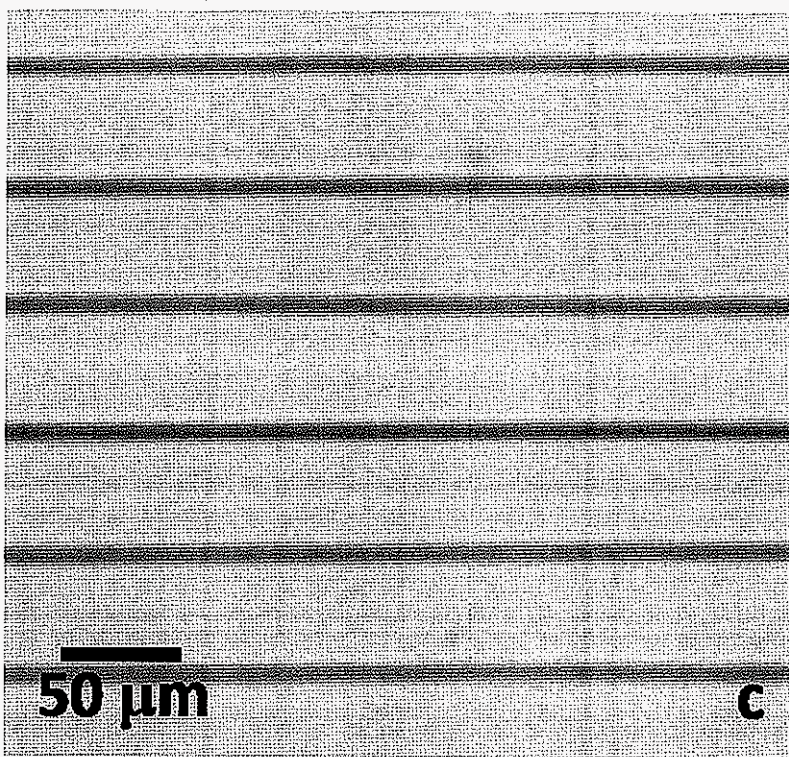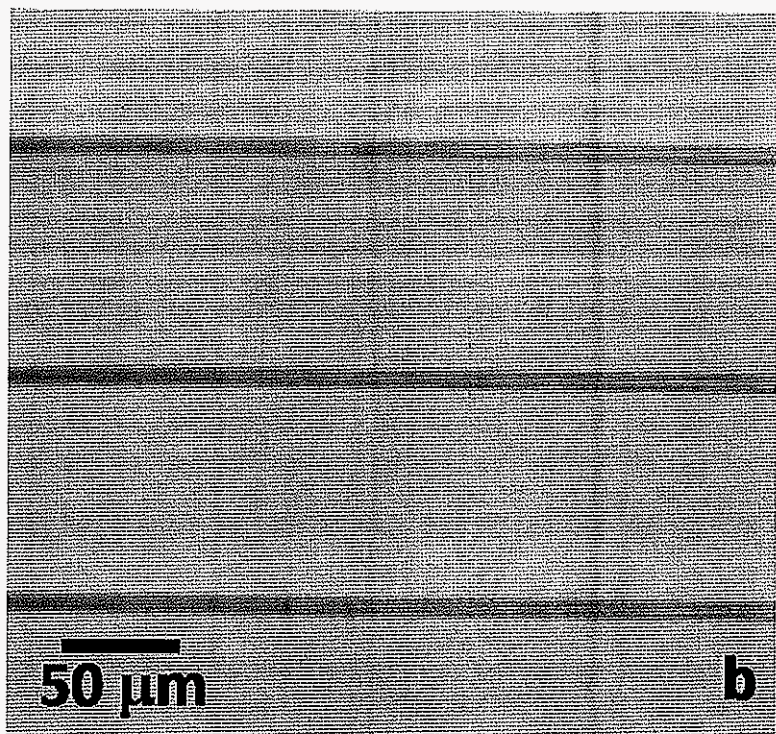**Figure 1.** Optical micrographs (10x magnification) of 5-100G (a), 5-100L (b), and 5-50L (c).
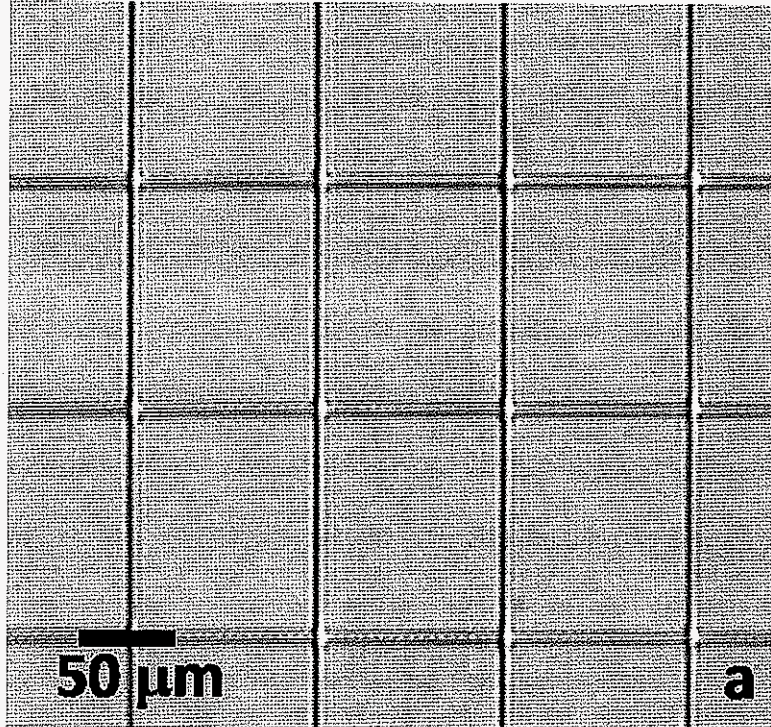
Figure 2. Profilometer scan across a single grid of a 5-50L CG-OTE.
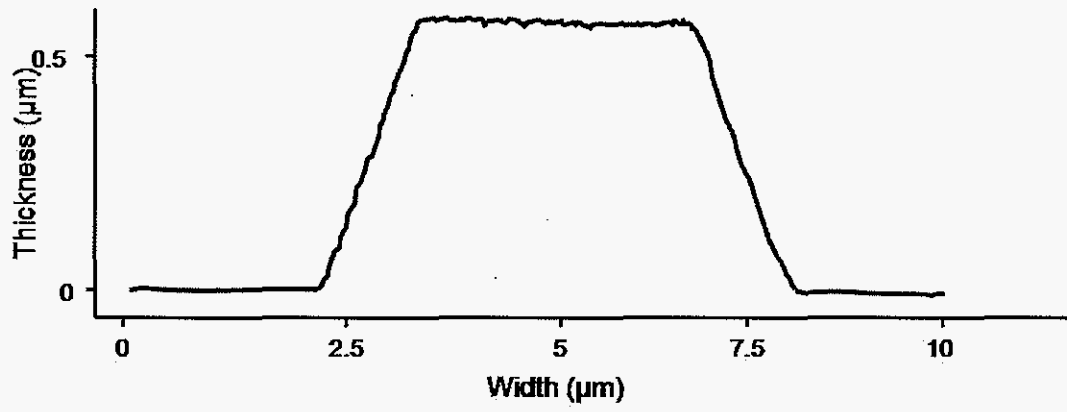
Figure 3. Optical micrographs (50x magnification) detailing crossing lines (a), and connection of line to surrounding PPF frame of 5-100G grid (b).
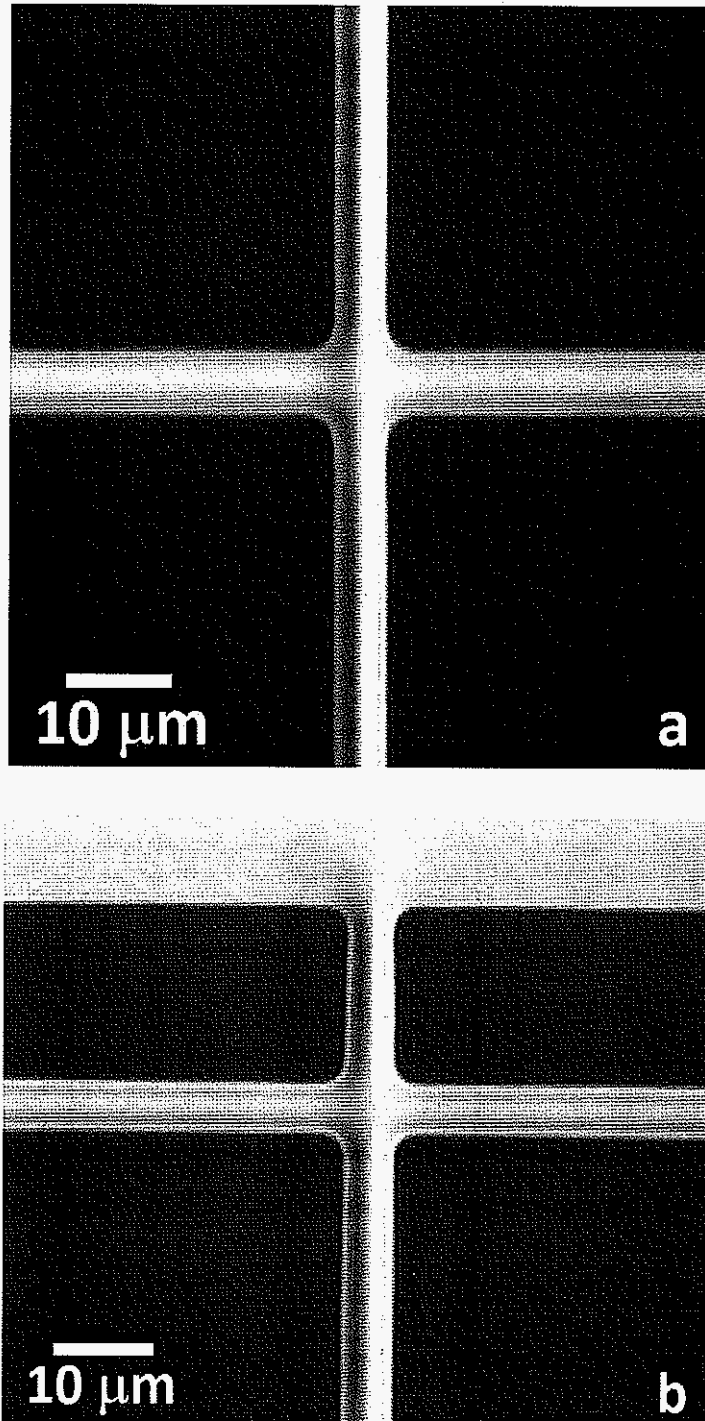
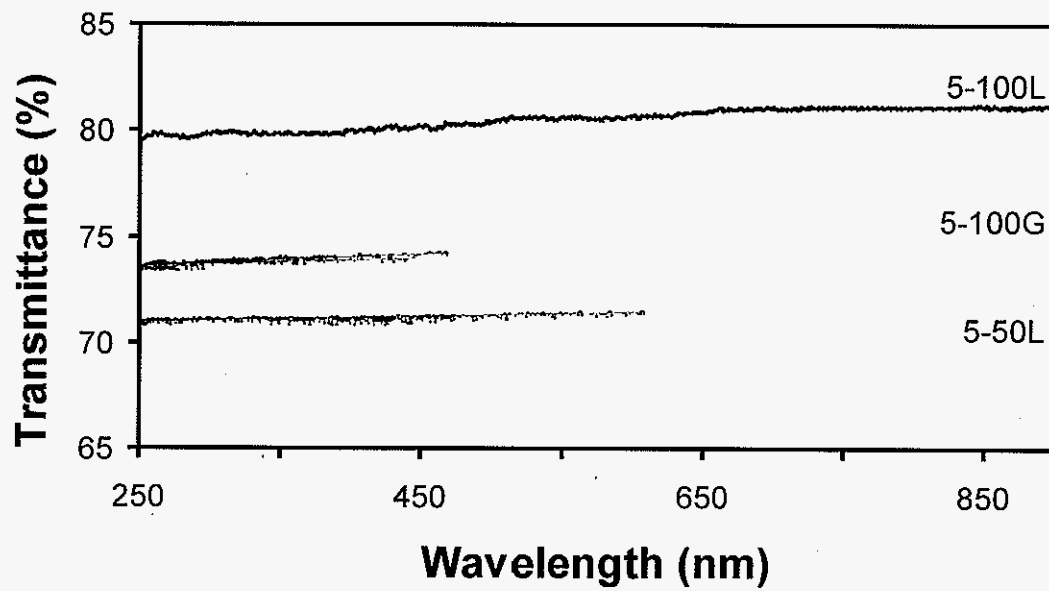**Figure 4.** Optical transparency of 5-100G, 5-100L, and 5-50L CG-OTEs.

Figure 5. Cyclic Voltammograms at 5-100G CG-OTE for: (a) 1mV/s for 1.0 mM hydroxymethylferrocene; and (b) 1.0 M potassium chloride at 1 mV/s.
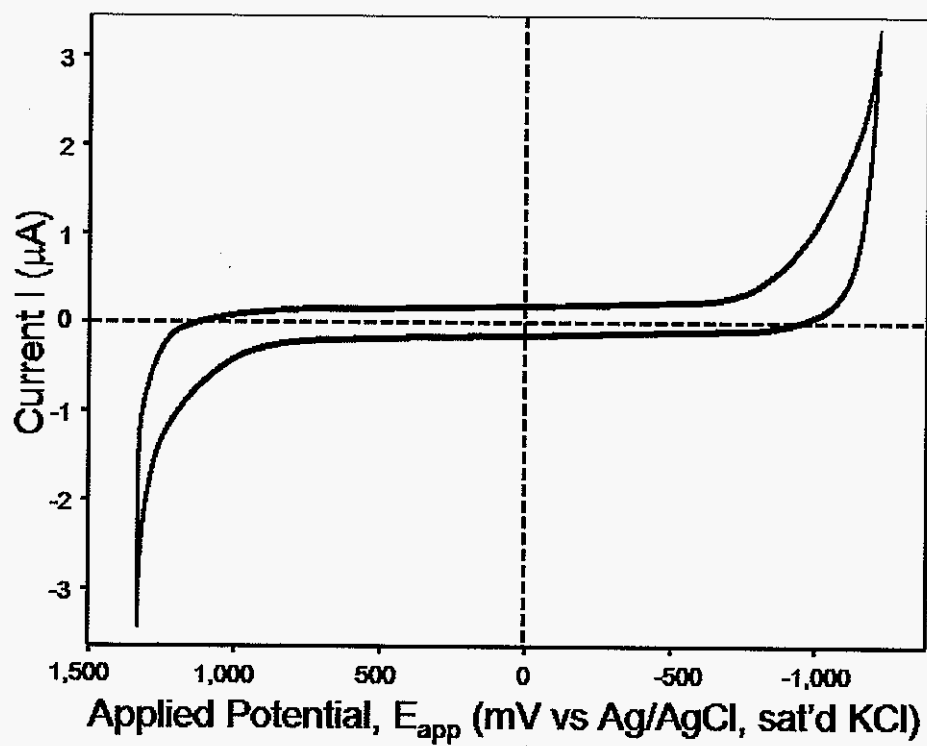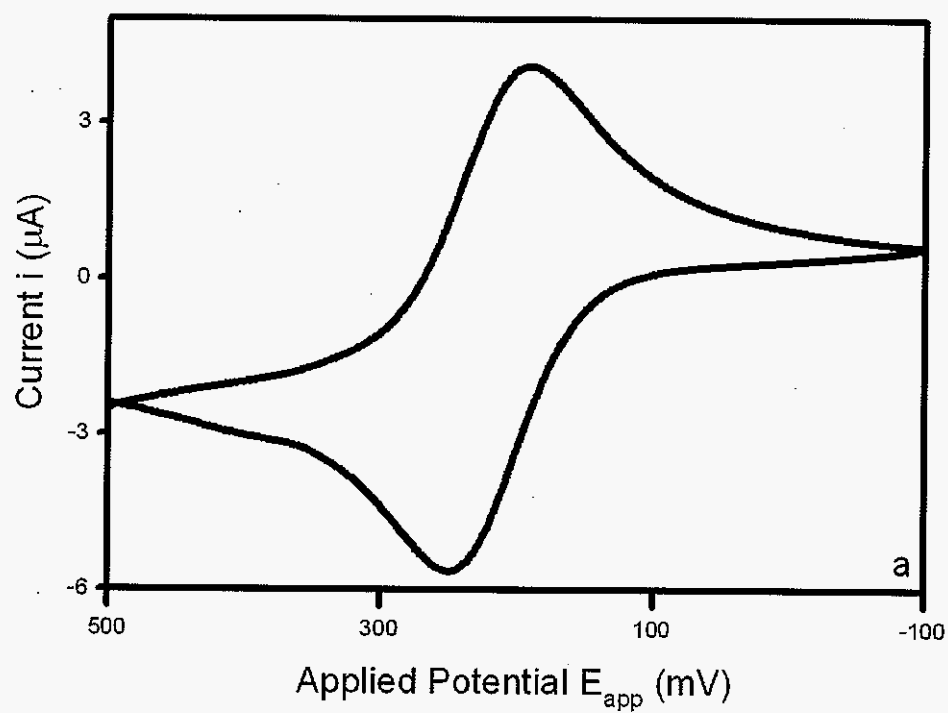
Figure 6. Absorbance of ferricyanide over time after the potential applied to a 10.0 mM solution of ferrocyanide (1.0 M KCl) is stepped to +600 mV (vs Ag/AgCl, sat'd KCl) at a 5-100G CG-OTE.
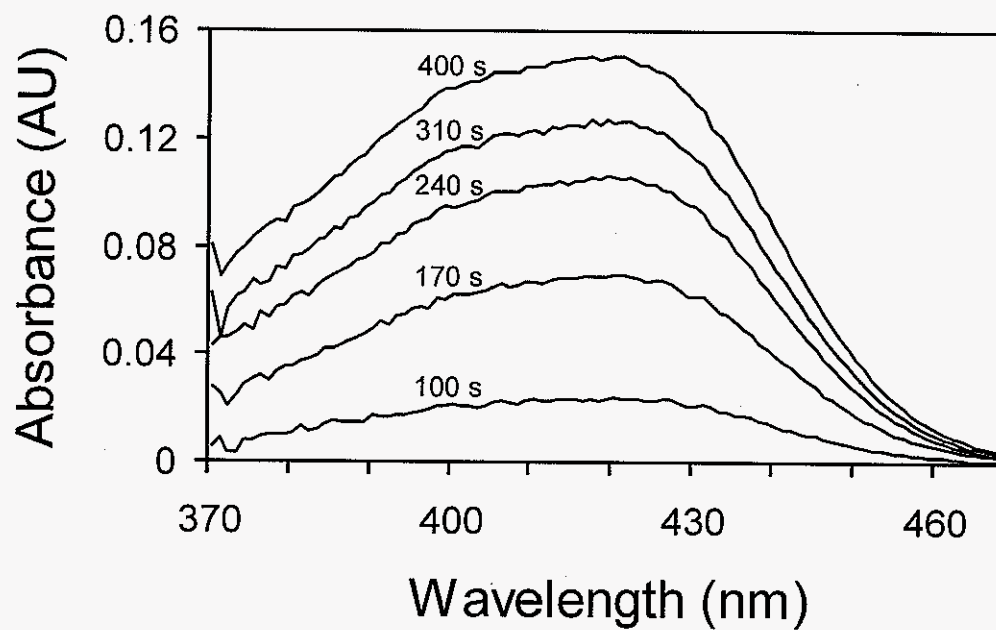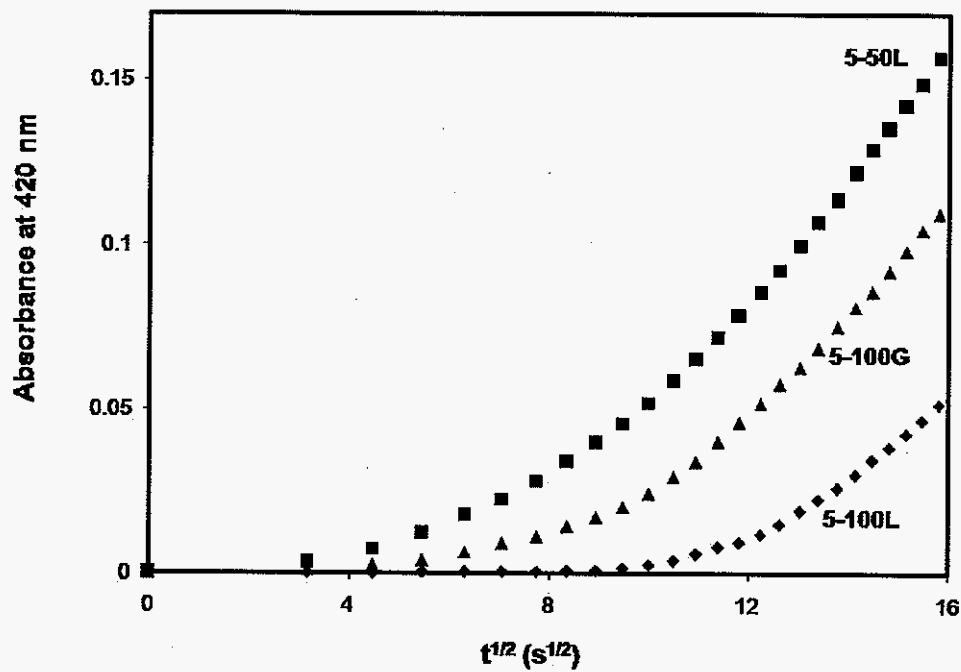
Figure 7. Absorbance of ferricyanide at 420 nm plotted versus the square root of time when a potential of +600 mV (vs Ag/AgCl, sat'd KCl) is applied to the electrode. Responses over a five-minute period for the three CG-OTEs are shown.

CHAPTER 5. CONCLUSIONS AND PROSPECTS

The fabrication of carbon based optically transparent electrodes (C-OTEs) provides an intriguing development in both electrochemistry and single molecule spectroscopy (SMS). Carbon electrodes offer a light weight and low cost alternative to platinum and gold while displaying a wide potential window and low background current. The ability to fabricate optically transparent carbon films opens the way to investigate this widely used electrode by single molecule spectroelectrochemistry (SMSEC).

The work presented in this thesis describes the inverse relationship between transparency and conductivity. The results indicate that 35-nm thick C-OTEs are optimal for spectroelectrochemical applications. Maintaining a transparency of 35% at a wavelength of 600 nm, the 35-nm thick C-OTEs display a resistivity of 2.4×10^{-3} Ωcm, a value comparable with that of the mostly widely used carbon electrode material, glassy carbon.

Incorporation of this conductive, optically transparent electrode material into total internal reflection microscopy (TIRFM) presents the novel merger of electrochemistry and SMS. This combination enabled us to study the behavior of single molecules within the electric double layer at the surface of carbon electrodes. Analytes used in our experiments include three different sizes of DNA, with the largest being λ-DNA (48.5 kbp), followed by HPV-16 (7.9 kbp), and a 1 kbp fraction of pBR322 DNA. We discovered that, depending on the applied potential, individual molecules can adsorb reversibly and irreversibly to the carbon surface. Adsorption sites are activated by applying a positive potential, with the number of adsorption sites increasing with increasing positive potential. Interestingly,

desorption does not occur to a significant extend when the potential is switched to a negative value. Once adsorption sites are created, the majority bind molecules irreversibly.

Future interrogations of carbon surface interactions using SMSEC will involve the use of smaller analyte molecules to gain better understanding of the retention characteristics of carbon as a stationary phase. We specifically plan to examine factors of possible importance in peak tailing and baseline drift in chromatographic experiments using electrochemically modulated liquid chromatography (EMLC). In addition, we also will investigate the effect of various surfaces to optimize reconditioning of the electrode material. Information gained from such experiments will enable optimal performance and increased lifetime of the carbonaceous packing material.

Our method for the manufacture of C-OTEs goes beyond the creation of transparent, thin-film carbon electrodes. Application of positive and negative photoresists not only presents a reliable and reproducible source for the starting material, but also enables the use of photolithographic patterning for forming intricate features and designs in such materials. Fabrication of multiple C-OTEs onto a single substrate can potentially increase throughput and decrease cost. In addition, the ability to pattern the photoresist led to the development of carbon grid optically transparent electrodes (CG-OTEs). To do so, we took advantage of producing and patterning thick photoresist films, which increased conductivity because the film thickness need not be restricted to tens of nanometers to realize transparency. In addition, our CG-OTEs possess increased transparency when compared to the C-OTEs. Electrochemical performance and transparency can further be altered by changing the dimensions of the grid, and line width, thickness, and spacing can be adjusted to meet the needs of various applications.